

Chapter 1

Quantum Metrology with Cold Atoms

Jiahao Huang, Shuyuan Wu, Honghua Zhong, and Chaohong Lee*

*State Key Laboratory of Optoelectronic Materials and Technologies,
School of Physics and Engineering, Sun Yat-Sen University, Guangzhou
510275, China
chleecn@gmail.com*

Quantum metrology is the science that aims to achieve precision measurements by making use of quantum principles. Attribute to the well-developed techniques of manipulating and detecting cold atoms, cold atomic systems provide an excellent platform for implementing precision quantum metrology. In this chapter, we review the general procedures of quantum metrology and some experimental progresses in quantum metrology with cold atoms. Firstly, we give the general framework of quantum metrology and the calculation of quantum Fisher information, which is the core of quantum parameter estimation. Then, we introduce the quantum interferometry with single and multi-particle states. In particular, for some typical multi-particle states, we analyze their ultimate precision limits and show how quantum entanglement could enhance the measurement precision beyond the standard quantum limit. Further, we review some experimental progresses in quantum metrology with cold atomic systems.

Contents

1. Quantum Metrology with Cold Atoms	1
<i>J. Huang, S. Wu, H. Zhong, and C. Lee</i>	
1. Introduction	2
2. Quantum Metrology	3
2.1. Measurement in Quantum Mechanics	3
2.2. General Procedure of Measurements	4
2.3. Parameter Estimation and Fisher Information	5
2.4. Quantum Fisher Information	8

*Corresponding author.

3. Quantum Interferometry with Single-Particle States	11
3.1. Mach-Zehnder interferometry	12
3.2. Ramsey interferometry	13
4. Quantum Interferometry with Multiparticle States	16
4.1. Spin coherent states	16
4.2. Spin squeezed states	20
4.3. NOON states	22
4.4. Entangled coherent states	24
4.5. Twin Fock states	25
5. Experimental Progresses	27
5.1. Bose-Einstein condensed atoms	27
5.1.1. Nonlinear interferometry with spin squeezed states	27
5.1.2. Twin matter-wave interferometry	32
5.2. Ultracold trapped ions	34
5.3. Cold atomic ensembles	35
6. Summary	37
References	38

1. Introduction

In recent years, the experimental techniques of manipulating cold atoms have been dramatically developed. Therefore, beyond exploring their quantum nature, it becomes possible to engineer cold atoms¹⁻³ for practical technology applications. Naturally, because of their robust quantum coherence and high controllability, cold atoms could be engineered to achieve high precision metrology at the level of quantum mechanics.⁴⁻⁸

Quantum metrology⁹⁻¹¹ aims to yield high measurement precisions by taking advantage of the quantum principles. A central goal of quantum metrology is how to enhance measurement precision with quantum resources such as entanglement and squeezing.⁹⁻²² For a multi-particle system of cold atoms, it has been demonstrated that quantum entanglement and spin squeezing can be prepared by employing intrinsic inter-atom interactions or laser induced artificial inter-atom interactions.²³⁻²⁵ Up to now, cold atoms have been widely used for implementing precision metrology, such as interferometers,²⁶⁻²⁸ gyroscopes,²⁹ quantum clocks,³⁰⁻³² magnetic field detectors³³⁻³⁵ and micro-gravity sensors.³⁶⁻³⁹

In this chapter, we review the recent progresses in quantum metrology with cold atoms. In Sec.2, we present the general framework of quantum metrology. In particular, we give the general procedure of measurement in quantum mechanics and the fundamental theory of parameter estimation. In Sec.3, we describe the basic principles of quantum interferometry with single-particle states, which includes the Ramsey interferometry and Mach-Zehnder interferometry. In Sec.4, we show the basic principles of quantum

interferometry with multiparticle states, such as, spin coherent states, spin squeezed states, NOON states, entangled coherent states and twin Fock states. In Sec.5, we mention some key experimental progresses in quantum metrology with various cold atomic systems, such as, ultracold trapped ions, cold atomic ensembles and Bose-Einstein condensed atoms. In the last section, we briefly summarize this review.

2. Quantum Metrology

2.1. *Measurement in Quantum Mechanics*

At the level of physics, a measurement is a physical process which estimates the quantity of a particular observable (or a physical parameter).⁴⁰ It plays a key role in most natural sciences and practical technologies. To compare different measurements, one has to specify magnitude, units and uncertainty for a particular measurement. The science of measurement is called as metrology.

The measurement process is governed by the laws of physics. Therefore, the measurement precision depends on both the performance imperfections and the fundamental limit imposed by the physical laws. The statistical fluctuations can be reduced by repeating the same measurement over times and averaging the results.^{11,41} According to the central limit theorem, for N repetitions of the same measurement, the statistical fluctuation scales as $1/\sqrt{N}$ which is called as the shot noise limit (SNL).⁹

In quantum mechanics, a measurement process is the action that determines a particular observable (or a physical parameter) of a quantum system. Quantum metrology aims to make high-precision measurements with quantum resources such as entanglement and squeezing. It has been demonstrated that quantum metrology could give better precision than the same measurement performed in a classical framework. For an example, the measurement precision of a Mach-Zehnder interferometer of N independent particles is limited by the standard quantum limit (SQL), which has the same scaling $1/\sqrt{N}$ for SNL. However, the measurement precision of a Mach-Zehnder interferometer of N entangled particles in the NOON state can reach the Heisenberg limit which has scaling $1/N$.⁴²⁻⁴⁴ Similar precision enhancements can also be obtained by other non-classical states such as spin squeezed states.⁴⁵

2.2. General Procedure of Measurements

Usually, a general measurement process includes three steps.^{10,11,46,47} First, prepare the probe into a desired initial state. Second, let the probe undergo a dynamical evolution dependent on the physical parameter to be measured. Third, read out the final state of the probe and estimate the physical parameter with the extracted information.

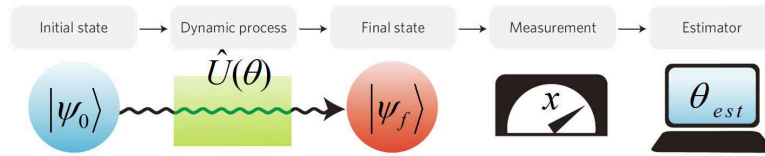


Fig. 1. The general procedure for a measurement process in quantum mechanics. An initial state is sent through a physical channel and evolves into the final state under a parameter-dependent dynamical process. Then, the final state is read out and the unknown parameter is estimated. From Ref. 47.

The density matrix of the initial state $|\psi_0\rangle$ for the probe can be expressed as,

$$\rho_0 = |\psi_0\rangle\langle\psi_0|. \quad (1)$$

The initial state is sent into a dynamical process dependent upon an unknown parameter θ to be measured. The initial state $|\psi_0\rangle$ evolves into the final state $|\psi(\theta)\rangle$ under the action of the parameter-dependent evolution operator $\hat{U}(\theta)$. If the evolution is unitary, the density matrix for the final state is given by,

$$\rho(\theta) = |\psi(\theta)\rangle\langle\psi(\theta)| = \hat{U}(\theta)\rho\hat{U}^\dagger(\theta). \quad (2)$$

Then, a measurement of a suitable observable \hat{O} is made on the final state $|\psi(\theta)\rangle$. To successfully extract the unknown parameter θ , the observable \hat{O} should have θ -dependent expectation values $\langle\hat{O}\rangle$.

If one has a prior knowledge of the evolution and the dependence of the observable expectation $\langle\hat{O}\rangle$ on the parameter θ , the information of the parameter θ can be revealed according to the measurement results of the observable \hat{O} . According to the error propagation formula, the standard deviation of the parameter is given by

$$\Delta\theta = \frac{\Delta\hat{O}}{\left|\frac{\partial\langle\hat{O}\rangle}{\partial\theta}\right|}, \quad (3)$$

where the standard deviation of the observable is defined as

$$\Delta\hat{O} = \sqrt{\langle\hat{O}^2\rangle - \langle\hat{O}\rangle^2} \quad (4)$$

with

$$\langle\hat{O}\rangle = \langle\psi(\theta)|\hat{O}|\psi(\theta)\rangle, \quad (5)$$

$$\langle\hat{O}^2\rangle = \langle\psi(\theta)|\hat{O}^2|\psi(\theta)\rangle. \quad (6)$$

It clearly shows that the standard deviation of the parameter $\Delta\theta$ is dependent on θ itself. In addition, the minimum standard deviation of the parameter $\Delta\theta$ corresponds to the maximum slope of the expectation value with respect to the parameter θ , $|\partial\langle\hat{O}\rangle/\partial\theta|$.

2.3. Parameter Estimation and Fisher Information

There are two typical kinds of parameter estimation. One is the local estimation, in which we have some prior knowledge about the parameter. The other is the global estimation, in which we don't have any prior knowledge about the parameter. If there is completely no prior knowledge about the parameter, the measurement results are just random to the observer and there is no necessary to estimate the precision of the parameter at all. Therefore, in most cases, the local estimation of an unknown parameter is implemented.⁴⁷⁻⁴⁹

In a realistic local estimation, we firstly measure a suitable observable x and then estimate the unknown parameter θ by an estimator function $\theta_{est} = T(x)$. Therefore, the uncertainty of the estimation (the measurement precision) is given by,^{50,51}

$$\delta\theta \equiv \frac{\theta_{est}}{|d\langle\theta_{est}\rangle/d\theta|} - \theta, \quad (7)$$

where θ_{est} and θ are the estimated and the actual values of the parameter, respectively. In the case of unbiased estimators, $\langle\theta_{est}\rangle = \theta$, the uncertainty is simply the standard deviation of the difference between the estimated and the actual value of the parameter. While in the case of random guesses, due to the average value of the estimated parameter is independent of θ , the derivative $\partial\langle\theta_{est}\rangle/\partial\theta = 0$ and the uncertainty diverges. This indicates that random guesses fail to estimate the parameter. Below, we concentrate our discussions on the unbiased estimators.

In one measurement of v times of identical experiments (or one experiment of v independent and identical probes), the measurement precision $\delta\theta$ is limited by the Cramér-Rao bound:^{50,52,53}

$$\delta\theta \geq \frac{1}{\sqrt{vF(\theta)}}. \quad (8)$$

Here, $F(\theta)$ is called as the Fisher information, which determines how precisely we can estimate a parameter θ .^{54,55} Obviously, the higher precision can be obtained with larger Fisher information.

For a continuum set of measurement data x , the Fisher information $F(\theta)$ is defined as

$$F(\theta) \equiv \int p(x|\theta) \left(\frac{\partial \ln[p(x|\theta)]}{\partial \theta} \right)^2 dx \quad (9)$$

with $p(x|\theta)$ denoting the conditional probability density of the measurement data x given the parameter θ . Thus $p(x|\theta)dx$ represents the conditional probability of the measurement data between x and $x+dx$ given the parameter θ .

For a discrete set of measurement data X_j , the Fisher information $F(\theta)$ is expressed as

$$F(\theta) \equiv \sum_j p(X_j|\theta) \left(\frac{\partial \ln[p(X_j|\theta)]}{\partial \theta} \right)^2 \quad (10)$$

with $p(X_j|\theta)$ denoting the conditional probability of the measurement data X_j given the parameter θ .

Now, we show why the Cramér-Rao bound gives the minimum uncertainty of the estimated parameter.^{49,50,53,56} Here, we only consider the measurement process of estimating a single continuous parameter θ with v identical experiments. The parameter θ is estimated by a function

$$\theta_{est} = T(x_1, x_2, \dots, x_v), \quad (11)$$

constructed from the measurement data (x_1, x_2, \dots, x_v) for the v experiments. As the v experiments are independent, the averaged value of θ_{est} is given as

$$\langle \theta_{est} \rangle = \int dx_1 \dots dx_v T(x_1, \dots, x_v) p(x_1|\theta) \dots p(x_v|\theta). \quad (12)$$

Obviously, the estimation function θ_{est} does not depend on the parameter θ , but the average $\langle \theta_{est} \rangle$ depends on the parameter θ .

Defining the deviation, $\Delta\theta_{est} = \theta_{est} - \langle\theta_{est}\rangle$, one can easily find

$$\int dx_1 \dots dx_v p(x_1|\theta) \dots p(x_v|\theta) \Delta\theta_{est} = 0. \quad (13)$$

According to the chain rule and $\partial\theta_{est}/\partial\theta = 0$, we yield its derivative with respect to the parameter θ ,

$$\sum_{i=1}^v \int dx_1 \dots dx_v p(x_1|\theta) \dots p(x_v|\theta) \frac{1}{p(x_i|\theta)} \frac{\partial p(x_i|\theta)}{\partial\theta} \Delta\theta_{est} - \frac{d\langle\theta_{est}\rangle}{d\theta} = 0. \quad (14)$$

Therefore, we have

$$\frac{d\langle\theta_{est}\rangle}{d\theta} = \int dx_1 \dots dx_v p(x_1|\theta) \dots p(x_v|\theta) \left(\sum_{i=1}^v \frac{\partial \ln [p(x_i|\theta)]}{\partial\theta} \right) \Delta\theta_{est}. \quad (15)$$

By applying the Cauchy-Schwarz inequality to the right-hand side of Eq. (15), one can obtain

$$\begin{aligned} \left(\frac{d\langle\theta_{est}\rangle}{d\theta} \right)^2 &\leq \int dx_1 \dots dx_v p(x_1|\theta) \dots p(x_v|\theta) \left(\sum_{i=1}^v \frac{\partial \ln [p(x_i|\theta)]}{\partial\theta} \right)^2 \\ &\quad \times \int dx_1 \dots dx_v p(x_1|\theta) \dots p(x_v|\theta) (\Delta\theta_{est})^2. \end{aligned} \quad (16)$$

Since

$$\int dx_i p(x_i|\theta) \frac{\partial \ln [p(x_i|\theta)]}{\partial\theta} = \int dx_i \frac{\partial p(x_i|\theta)}{\partial\theta} = \frac{d}{d\theta} \int dx_i p(x_i|\theta) = 0, \quad (17)$$

all cross terms in the right-hand side of Eq. (16) vanish, and the square of the sum reduces to

$$\begin{aligned} \left(\frac{d\langle\theta_{est}\rangle}{d\theta} \right)^2 &\leq \int dx_1 \dots dx_v p(x_1|\theta) \dots p(x_v|\theta) \sum_{i=1}^v \left(\frac{\partial \ln [p(x_i|\theta)]}{\partial\theta} \right)^2 \\ &\quad \times \int dx_1 \dots dx_v p(x_1|\theta) \dots p(x_v|\theta) (\Delta\theta_{est})^2. \end{aligned} \quad (18)$$

Denoting $\langle(\Delta\theta_{est})^2\rangle = \int dx_1 \dots dx_v p(x_1|\theta) \dots p(x_v|\theta) (\Delta\theta_{est})^2$, we have

$$\begin{aligned} \left(\frac{d\langle\theta_{est}\rangle}{d\theta} \right)^2 &\leq \langle(\Delta\theta_{est})^2\rangle \\ &\quad \times \int dx_1 \dots dx_v p(x_1|\theta) \dots p(x_v|\theta) \sum_{i=1}^v \left(\frac{\partial \ln [p(x_i|\theta)]}{\partial\theta} \right)^2 \end{aligned} \quad (19)$$

As the measurement data (x_1, x_2, \dots, x_v) are independent and the integral for each x_v has the same form of the Fisher information Eq. (9), the above inequality becomes

$$\langle (\Delta\theta_{est})^2 \rangle vF(\theta) \geq \left(\frac{d \langle \theta_{est} \rangle}{d\theta} \right)^2. \quad (20)$$

It can also be written in the form of

$$\frac{\langle (\Delta\theta_{est})^2 \rangle}{(d \langle \theta_{est} \rangle / d\theta)^2} \geq \frac{1}{vF(\theta)}. \quad (21)$$

To show how the estimated parameter is close to the actual one, the uncertainty given in Eq. (7) should be calculated. In general, we regard the expectation of the unknown estimated parameter over many times as the actual one, that is, $\langle \theta_{est} \rangle = \theta$. Therefore, the average of the square of Eq. (7) is given as

$$\langle (\delta\theta)^2 \rangle = \frac{\langle \Delta\theta_{est}^2 \rangle}{(d \langle \theta_{est} \rangle / d\theta)^2} + \langle \delta\theta \rangle^2. \quad (22)$$

Substituting Eq. (22) into Eq. (21), the inequality reads as

$$\langle (\delta\theta)^2 \rangle \geq \frac{1}{vF(\theta)} + \langle \delta\theta \rangle^2. \quad (23)$$

As $\langle \theta_{est} \rangle = \theta$, the derivative $d \langle \theta_{est} \rangle / d\theta = 1$, $\langle \delta\theta \rangle^2 = 0$, and $\langle (\delta\theta)^2 \rangle$ reduces to the variance $\langle (\Delta\theta)^2 \rangle$. That is, the above inequality becomes

$$\langle (\delta\theta)^2 \rangle = \langle (\Delta\theta)^2 \rangle \geq \frac{1}{vF(\theta)}, \quad (24)$$

whose square root

$$\sqrt{\langle (\delta\theta)^2 \rangle} = \sqrt{\langle (\Delta\theta)^2 \rangle} \geq \frac{1}{\sqrt{vF(\theta)}}, \quad (25)$$

gives the so-called Cramér-Rao bound.

2.4. Quantum Fisher Information

In quantum mechanics, a generalized measurement can be described by a set of Hermitian operators $\hat{E}(x)$, which are Positive-Operator Valued Measures (POVM).⁵⁷ The quantity x is the measurement data which corresponds to the measurement values of the observable \hat{O} in Sec. 2.2. The operators $\hat{E}(x)$ satisfy,

$$\hat{E}(x) \geq 0, \int dx \hat{E}(x) = \mathbf{1}, \quad (26)$$

where $\mathbf{1}$ is the identity operator. This relation ensures non-negative probabilities and unitary total probability.

The probability of getting the measurement data x on a state $|\psi\rangle$ is given by,

$$P(x) = \langle \psi | \hat{E}(x) | \psi \rangle = \text{Tr}[\rho \hat{E}(x)], \quad (27)$$

where $\rho = |\psi\rangle\langle\psi|$ is the density matrix.

Therefore, by making a measurement on the final state, according to Eq. (27), one can obtain the conditional probability of the measurement result x given the parameter θ ,

$$P(x|\theta) = \langle \psi(\theta) | \hat{E}(x) | \psi(\theta) \rangle = \text{Tr}[\rho(\theta) \hat{E}(x)]. \quad (28)$$

Clearly, Eq. (25) and Eq. (28) indicate that the uncertainty $\delta\theta$ is inversely proportional to the Fisher information $F(\theta)$. According to the definition of the Fisher information, one can find that $F(\theta)$ is a function of the conditional probability $p(x|\theta)$ which depends on the final state $|\psi(\theta)\rangle$ and the form of $\hat{E}(x)$. Therefore, to optimize the Fisher information, we need to construct a suitable state and measure a suitable observable. Further, for a given final state, the Fisher information can be maximized by trying different measurement strategies. The maximum of Fisher information through out all possible quantum measurement strategies is called as the quantum Fisher information,^{44,58}

$$F_Q(\theta) \equiv \max_{\{\hat{E}(x)\}} F[\rho(\theta); \{\hat{E}(x)\}], \quad (29)$$

and the corresponding Cramér-Rao bound is called as the quantum Cramér-Rao bound,⁵¹

$$\sqrt{\langle (\delta\theta)^2 \rangle} \geq \frac{1}{\sqrt{v F_Q(\theta)}}. \quad (30)$$

Below, as an example, we show how to derive the quantum Fisher information and quantum Cramér-Rao bound for a pure state under a unitary evolution.⁵⁶ Their explicit expressions can be obtained without the knowledge of measurement $\hat{E}(x)$. Here, we consider a probe in the initial state $|\psi_0\rangle$ undergoing an evolution described the operator $\hat{U}(\theta) = \exp(-i\hat{H}\theta)$ with the θ -independent generator \hat{H} . Inserting Eq. (2) into Eq. (28), we

obtain

$$\begin{aligned}
\frac{\partial p(x|\theta)}{\partial \theta} &= \left[\frac{d}{d\theta} \langle \psi(\theta) | \hat{E}(x) | \psi(\theta) \rangle + \langle \psi(\theta) | \hat{E}(x) \left[\frac{d}{d\theta} | \psi(\theta) \rangle \right] \right], \\
&= i \langle \psi(\theta) | \hat{H} \hat{E}(x) | \psi(\theta) \rangle - i \langle \psi(\theta) | \hat{E}(x) \hat{H} | \psi(\theta) \rangle, \\
&= i \langle \psi(\theta) | [\hat{H}, \hat{E}(x)] | \psi(\theta) \rangle, \\
&= 2Im \left[\langle \psi(\theta) | \hat{H} \hat{E}(x) | \psi(\theta) \rangle \right].
\end{aligned} \tag{31}$$

Inserting an arbitrary real function $G(\theta)$ into Eq. (31), we have

$$\frac{\partial p(\theta|x)}{\partial \theta} = 2Im \left\{ \langle \psi(\theta) | [\hat{H} - G(\theta)] \hat{E}(x) | \psi(\theta) \rangle \right\}, \tag{32}$$

and so that

$$\begin{aligned}
\left(\frac{\partial p(x|\theta)}{\partial \theta} \right)^2 &= 4Im^2 \left\{ \langle \psi(\theta) | [\hat{H} - G(\theta)] \hat{E}(x) | \psi(\theta) \rangle \right\}, \\
&\leq 4 |\langle \psi(\theta) | [\hat{H} - G(\theta)] \hat{E}(x) | \psi(\theta) \rangle|^2, \\
&\leq 4 \langle \psi(\theta) | \hat{E}(x) | \psi(\theta) \rangle \langle \psi(\theta) | [\hat{H} - G(\theta)] \hat{E}(x) [\hat{H} - G(\theta)] | \psi(\theta) \rangle, \\
&= 4p(x|\theta) \langle \psi(\theta) | [\hat{H} - G(\theta)] \hat{E}(x) [\hat{H} - G(\theta)] | \psi(\theta) \rangle.
\end{aligned} \tag{33}$$

Therefore, one can obtain

$$\begin{aligned}
F(\theta) &= \int dx \frac{1}{p(x|\theta)} \left[\frac{\partial p(x|\theta)}{\partial \theta} \right]^2, \\
&\leq 4 \int dx \langle \psi(\theta) | [\hat{H} - G(\theta)] \hat{E}(x) [\hat{H} - G(\theta)] | \psi(\theta) \rangle, \\
&= 4 \langle \psi(\theta) | [\hat{H} - G(\theta)]^2 | \psi(\theta) \rangle.
\end{aligned} \tag{34}$$

If $G(\theta) = \langle \psi_0 | \hat{H} | \psi_0 \rangle$, due to $\langle \hat{H} \rangle = \langle \psi_0 | \hat{H} | \psi_0 \rangle = \langle \psi(\theta) | \hat{H} | \psi(\theta) \rangle$, the Fisher information attain its minimum and the inequality reads as

$$F(\theta) \leq 4 \langle \psi_0 | (\Delta \hat{H})^2 | \psi_0 \rangle \tag{35}$$

with $\Delta \hat{H} = \hat{H} - \langle \hat{H} \rangle$. Therefore, the quantum Fisher information for a pure state can be defined as^{47,59,60}

$$F_Q(\theta) = 4 \langle \psi_0 | (\Delta \hat{H})^2 | \psi_0 \rangle, \tag{36}$$

which is a function of the generator \hat{H} and the initial state $|\psi_0\rangle$, but not a function of the final state $|\psi(\theta)\rangle$. By using $|\psi(\theta)\rangle = \hat{U}|\psi_0\rangle =$

$\exp(-i\hat{H}\theta)|\psi_0\rangle$ and $|\psi'(\theta)\rangle = d|\psi(\theta)\rangle/d\theta = -i\hat{H}|\psi(\theta)\rangle$, $F_Q(\theta)$ can also be written as

$$F_Q(\theta) = 4 \left[\langle \psi'(\theta) | \psi'(\theta) \rangle - |\langle \psi'(\theta) | \psi(\theta) \rangle|^2 \right], \quad (37)$$

which is a function of the final state $|\psi(\theta)\rangle$ and its derivative with respect to θ , but not a function of the initial state $|\psi_0\rangle$.

The quantum Fisher information provides a powerful tool for parameter estimation only dependent on the state of the system but not on the form of measurement.^{61–63} As long as the initial state and the final state of the probe after the parameter-dependent evolution are known, one can immediately predict the minimum uncertainty of the parameter in theory. Generally speaking, the quantum Cramér-Rao bound is the theoretical minimum of the parameter uncertainty, and the parameter uncertainty in realistic measurements may be larger.

3. Quantum Interferometry with Single-Particle States

Interferometry is an important and most used method for implementing measurements.^{64–67} Interferometry via quantum states includes three key steps: (i) splitting the initial state into two modes, (ii) undergoing a period of free evolution and (iii) recombining two modes for readout. There are two typical types of interferometry. One is the Mach-Zehnder interferometry, which has extensive applications in phase shift measurements.^{68,69} The other is the Ramsey interferometry, which has been widely used in atomic-molecular experiments for precision spectroscopy and measurement.^{70–72} In this section, we briefly introduce these two kinds of interferometry with single-particle states.

It is well known that a two-mode (or two-level) quantum particle can be regarded as a spin- $\frac{1}{2}$ particle, which can be described by the three Pauli matrices $\hat{\sigma}_x$, $\hat{\sigma}_y$ and $\hat{\sigma}_z$.^{73,74} The two eigenstates $|\uparrow\rangle$ and $|\downarrow\rangle$ obey $\frac{\sigma_z}{2}|\uparrow\rangle = +\frac{1}{2}|\uparrow\rangle$ and $\frac{\sigma_z}{2}|\downarrow\rangle = -\frac{1}{2}|\downarrow\rangle$ and an arbitrary pure state can be written as $|\theta, \varphi\rangle = e^{i\gamma} \left(\sin \frac{\theta}{2} |\uparrow\rangle + \cos \frac{\theta}{2} e^{i\varphi} |\downarrow\rangle \right)$ with the common phase γ . The factor $e^{i\gamma}$ has no observable effects, thus the pure states $|\theta, \varphi\rangle$ with different values of γ are represented by the same classical spin $(S_x, S_y, S_z) = \frac{1}{2}(\sin \theta \cos \varphi, \sin \theta \sin \varphi, \cos \theta)$ in the Bloch sphere. Where, the longitudinal component $S_z = \cos \theta = \frac{1}{2}(\cos^2 \frac{\theta}{2} - \sin^2 \frac{\theta}{2})$ stands for the half population difference between the two eigenstates, and the transverse components (S_x, S_y) stand for the quantum coherence between the

two modes. This means that the polar angle θ reflects the polarization information, while the azimuthal angle φ corresponds to coherence.

3.1. Mach-Zehnder interferometry

A conventional Mach-Zehnder interferometer is composed of two beam splitters and two propagation paths.^{68,75–77} A collimated beam of single particles is divided into two parts by a 50:50 beam splitter. Then the two parts pass through two different spatial paths and accumulate a relative phase shift between the two parts. At last, the two parts are recombined for interference via another 50:50 beam splitter. The phase difference can be extracted from the interference fringe.⁷⁸ The schematic diagram is shown in Fig. 2.

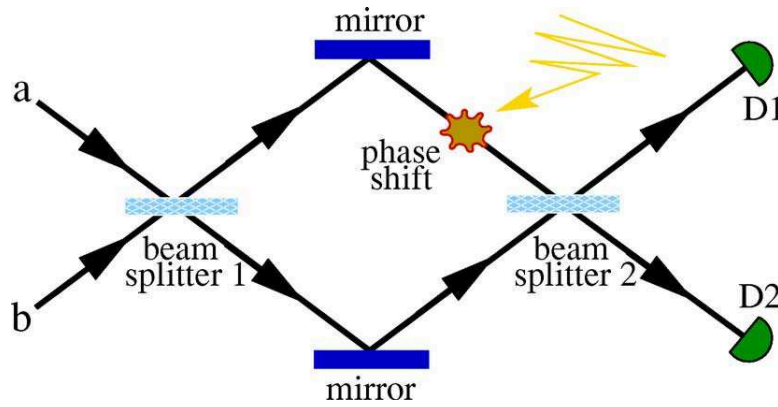


Fig. 2. Schematic diagram of a Mach-Zehnder interferometer. Single atoms/photons enter the input ports, combine in the first beam splitter, evolve in the two paths, recombine via the second beam splitter and are finally detected in D1 and D2. The phase shift is inferred from the number of atoms or photons measured in each output port. From Ref. 79.

Suppose an atom incidents in the input port a , that is, the initial state of the atom is prepared in mode $|a\rangle$. The first beam splitter transforms the input state into an equal superposition state of the two involved modes $|a\rangle$ and $|b\rangle$,

$$|\psi_{in}\rangle = \hat{T}|a\rangle = \frac{1}{\sqrt{2}}(|a\rangle + |b\rangle), \quad (38)$$

with the transformation matrix,

$$\hat{T} = \frac{1}{\sqrt{2}} \begin{pmatrix} 1 & 1 \\ 1 & -1 \end{pmatrix}. \quad (39)$$

Then the two modes propagate along different paths and accumulate a relative phase shift φ . That is, before entering into the second beam splitter, the state reads as

$$|\psi_{out}\rangle = \frac{1}{\sqrt{2}}(|a\rangle + e^{i\varphi}|b\rangle). \quad (40)$$

The second beam splitter recombines the two paths and the state is transformed into,

$$|\psi_f\rangle = \hat{T}\psi_{out} = \frac{1}{\sqrt{2}}[(1 + e^{i\varphi})|a\rangle + (1 - e^{i\varphi})|b\rangle]. \quad (41)$$

At last, the output state is detected by $D1$ and $D2$, which give $p(a|\varphi) = \cos^2(\varphi/2)$ for the probability of the atom in $|a\rangle$ and $p(b|\varphi) = \sin^2(\varphi/2)$ for the probability of the atom in $|b\rangle$.

From Eq. (10), the Fisher information for the above single-atom Mach-Zehnder interferometry can be obtained,

$$\begin{aligned} F(\varphi) &= \frac{1}{p(a|\varphi)} \left[\frac{\partial p(a|\varphi)}{\partial \varphi} \right]^2 + \frac{1}{p(b|\varphi)} \left[\frac{\partial p(b|\varphi)}{\partial \varphi} \right]^2, \\ &= \sin^2 \varphi + \cos^2 \varphi = 1. \end{aligned} \quad (42)$$

Therefore, the minimal uncertainty of the relative phase is given as,

$$\delta\varphi = \frac{1}{\sqrt{F(\varphi)}} = 1. \quad (43)$$

Repeating the experiment N times, the uncertainty of the relative phase reads as,

$$\delta\varphi = \frac{1}{\sqrt{NF(\varphi)}} = \frac{1}{\sqrt{N}}, \quad (44)$$

which attains the so-called standard quantum limit (SQL).

3.2. Ramsey interferometry

The conventional Ramsey interferometry consists of two $\frac{\pi}{2}$ pulses and a free evolution process. In comparison with Mach-Zehnder interferometry, the two $\frac{\pi}{2}$ pulses act as the two beam splitters and the free evolution accumulate the relative phase between the two involved levels.^{80–83}

We consider a two-level atom, which is initially prepared in its ground state $|\downarrow\rangle$. Without loss of generality, we assume that the eigen-energies for the ground state $|\downarrow\rangle$ and the excited state $|\uparrow\rangle$ are $-\frac{\omega_0}{2}$ and $+\frac{\omega_0}{2}$, respectively. The first $\frac{\pi}{2}$ pulse is applied and the state becomes

$$|\psi_{in}\rangle = \frac{1}{\sqrt{2}}(|\downarrow\rangle + |\uparrow\rangle), \quad (45)$$

which is an equal-probability superposition of the ground state $|\downarrow\rangle$ and the excited state $|\uparrow\rangle$. Then, the system undergoes a free evolution. In which, the ground state $|\downarrow\rangle$ accumulates a negative phase $-\frac{\varphi}{2}$, while the excited state $|\uparrow\rangle$ accumulates a positive phase $+\frac{\varphi}{2}$. Therefore, the state after the free evolution reads as,

$$|\psi_{out}\rangle = \frac{1}{\sqrt{2}}(e^{-i\varphi/2}|\downarrow\rangle + e^{+i\varphi/2}|\uparrow\rangle). \quad (46)$$

At last, the second $\frac{\pi}{2}$ pulse is applied and the final state is measured. The probability of the atom in the ground state $|\downarrow\rangle$ reads as,

$$p(\downarrow|\varphi) = \frac{1 + \cos\varphi}{2} = \cos^2\frac{\varphi}{2}, \quad (47)$$

and the probability of the atom in the excited state $|\uparrow\rangle$ reads as,

$$p(\uparrow|\varphi) = 1 - p(\downarrow|\varphi) = \frac{1 - \cos\varphi}{2} = \sin^2\frac{\varphi}{2}. \quad (48)$$

The relative phase φ can be estimated from the probability $p(\downarrow|\varphi)$ or $p(\uparrow|\varphi)$. From Eq. (10), one can obtain the Fisher information for the above single-atom Ramsey interferometry,

$$\begin{aligned} F(\varphi) &= \frac{1}{p(\downarrow|\varphi)} \left[\frac{\partial p(\downarrow|\varphi)}{\partial \varphi} \right]^2 + \frac{1}{p(\uparrow|\varphi)} \left[\frac{\partial p(\uparrow|\varphi)}{\partial \varphi} \right]^2, \\ &= \sin^2\varphi + \cos^2\varphi = 1. \end{aligned} \quad (49)$$

Therefore, the minimal uncertainty of the relative phase is given by,

$$\delta\varphi = \frac{1}{\sqrt{F(\varphi)}} = 1. \quad (50)$$

Repeating the experiment N times, the uncertainty of the relative phase is limited by the standard quantum limit,

$$\delta\varphi = \frac{1}{\sqrt{NF(\varphi)}} = \frac{1}{\sqrt{N}}. \quad (51)$$

In the Bloch sphere, the initial state $|\downarrow\rangle$ is denoted by a spin vector pointing from the origin to the south pole. The first $\frac{\pi}{2}$ pulse rotates the

state an angle $\frac{\pi}{2}$ around the y -axis. The free evolution rotates the state an angle φ around the z -axis. The second $\frac{\pi}{2}$ pulse rotates the state an angle $\frac{\pi}{2}$ around the y -axis. Lastly, the angle between the spin vector for the final state and the negative z -axis is just the angle φ .

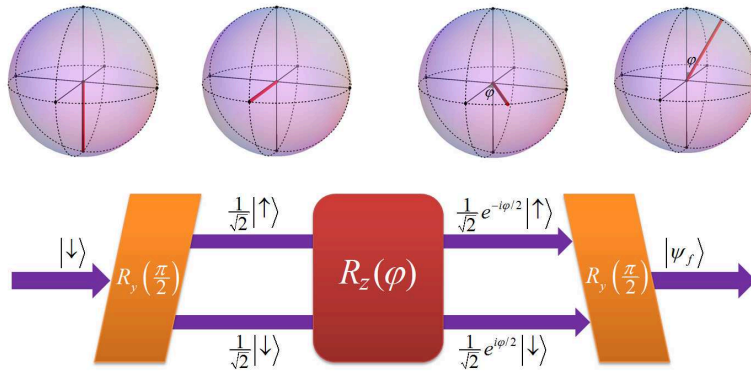


Fig. 3. Schematic diagram for a single-atom Ramsey interferometer. The two $\frac{\pi}{2}$ pulses and the free evolution are specific rotations in the geometrical representation via the Bloch sphere.

The state evolution from the initial state to the final state can be described by,

$$|\psi_f\rangle = \hat{U}|\psi_0\rangle, \quad (52)$$

with the propagation operator

$$\hat{U} = \exp(-i\frac{\pi}{2}\hat{S}_y) \exp(-i\varphi\hat{S}_z) \exp(-i\frac{\pi}{2}\hat{S}_y). \quad (53)$$

Here, the spin operators are defined as $\hat{S}_{x,y,z} = \frac{1}{2}\hat{\sigma}_{x,y,z}$. Thus the expectation value for the final state reads as,

$$\langle\hat{S}_z\rangle_f = \langle\psi_f|\hat{S}_z|\psi_f\rangle = \langle\psi_0|\hat{U}^\dagger\hat{S}_z\hat{U}|\psi_0\rangle. \quad (54)$$

Substituting Eq. (53) into Eq. (54), we have

$$\langle\hat{S}_z\rangle_f = -\cos\varphi\langle\hat{S}_z\rangle_0 + \sin\varphi\langle\hat{S}_y\rangle_0 \quad (55)$$

and

$$\begin{aligned} (\Delta\hat{S}_z)_f^2 &= (\Delta\hat{S}_z)_0^2 \cos^2\varphi + (\Delta\hat{S}_y)_0^2 \sin^2\varphi \\ &\quad - \sin\varphi \cos\varphi \langle\hat{S}_z\hat{S}_y + \hat{S}_y\hat{S}_z\rangle \end{aligned} \quad (56)$$

As the initial state $|\psi_0\rangle = |\downarrow\rangle_0$, we have

$$\langle \hat{S}_z \rangle_0 = \frac{1}{2}, \langle \hat{S}_z^2 \rangle_0 = \langle \hat{S}_y^2 \rangle_0 = \langle \hat{S}_x^2 \rangle_0 = \frac{1}{4}, \langle \hat{S}_x \rangle_0 = \langle \hat{S}_y \rangle_0 = 0.$$

Thus one can immediately obtain

$$\left(\Delta \hat{S}_z \right)_f = \frac{1}{2} \sin \varphi \quad (57)$$

According to Eq. (3), the standard deviation of φ is given by,

$$\Delta \varphi = \frac{\left(\Delta \hat{S}_z \right)_f}{\left| \partial \langle \hat{S}_z \rangle_f / \partial \varphi \right|} = 1, \quad (58)$$

which agrees with the minimal uncertainty given by the Fisher information Eq. (50). Repeating the measurement N times, the uncertainty can reach the standard quantum limit $\Delta \varphi \sim \frac{1}{\sqrt{N}}$.

4. Quantum Interferometry with Multiparticle States

In this section, we discuss the quantum interferometry with multiparticle states. There are many different types of multiparticle states that have been used to implement quantum interferometry.⁸⁴⁻⁹⁴ Here, we concentrate our discussions on spin coherent states, spin squeezed states, NOON states, entangled coherent states and twin Fock states.

4.1. Spin coherent states

For an ensemble of N two-level particles, which can be regarded as N identical spin- $\frac{1}{2}$ particles, one can mathematically describe the system by a collective spin of length $J = \frac{N}{2}$.^{13,95} Such a spin- J system is characterized by three collective spin operators \hat{J}_x , \hat{J}_y and \hat{J}_z which are defined as the sum of spin operators of spin- $\frac{1}{2}$ spin operators \hat{S}_x , \hat{S}_y and \hat{S}_z ,

$$\hat{J}_i = \sum_{l=1}^N \hat{S}_i^{(l)}, \quad (i = x, y, z). \quad (59)$$

By using the Schwinger representation,⁹⁶ the collective spin operators can be written in form of

$$\hat{J}_x = \frac{1}{2} \left(\hat{a}^\dagger \hat{b} + \hat{b}^\dagger \hat{a} \right), \quad (60)$$

$$\hat{J}_y = \frac{i}{2} (\hat{a}^\dagger \hat{b} - \hat{b}^\dagger \hat{a}) \quad (61)$$

$$\hat{J}_z = \frac{1}{2} (\hat{b}^\dagger \hat{b} - \hat{a}^\dagger \hat{a}) \quad (62)$$

in which the bosonic operators \hat{a}^\dagger (\hat{b}^\dagger) and \hat{a} (\hat{b}) denote the creation and annihilation operators for particles in $|\downarrow\rangle$ ($|\uparrow\rangle$), respectively.

The three collective spin operators obey the commutation relation,

$$[\hat{J}_\alpha, \hat{J}_\beta] = i\hbar \epsilon_{\alpha\beta\gamma} \hat{J}_\gamma \quad (\alpha, \beta, \gamma = x, y, z) \quad (63)$$

where ϵ_{ijk} is the Levi-Civita symbol. Below, without loss of generality, we use the unit of $\hbar = 1$. Thus, the collective spin operators obey the uncertainty relation,

$$\Delta \hat{A} \Delta \hat{B} \geq \frac{1}{2} |\langle [\hat{A}, \hat{B}] \rangle|, \quad (64)$$

where $\Delta \hat{A}$ and $\Delta \hat{B}$ are standard deviations. Inserting Eq. (63) into Eq. (64), one can obtain the uncertainty relation

$$\Delta \hat{J}_\alpha \Delta \hat{J}_\beta \geq \frac{1}{2} |\langle \hat{J}_\gamma \rangle|, \quad (65)$$

for the three collective spin operators.

Coherent spin states (CSS) are the most ‘classical like’ pure quantum states of N spin- $\frac{1}{2}$ particles that polarize in the same single-particle state.⁹⁷ Therefore, an arbitrary CSS can be expressed as

$$|\theta, \varphi\rangle_{CSS} = \otimes_{l=1}^N \left[\sin(\theta/2) e^{-i\varphi} |\uparrow\rangle_l + \cos(\theta/2) e^{i\varphi/2} |\downarrow\rangle_l \right], \quad (66)$$

which can be generated from the all-spin-down state $|0, 0\rangle_{CSS} = \otimes_{l=1}^N |\downarrow\rangle_l$ by a unitary rotation with angles θ and φ . The direction from the origin to the point (θ, φ) on the Bloch sphere corresponds to the direction of the mean total spin $\langle J \rangle$, which is called as the mean spin direction (MSD).

One can also express a CSS in terms of the Dicke basis $|J, m\rangle$. The Dicke states are defined by the common eigenstates of \hat{J}^2 and \hat{J}_z : $\hat{J}^2 |J, m\rangle = J(J+1) |J, m\rangle$ and $\hat{J}_z |J, m\rangle = m |J, m\rangle$. Here, we have $J = N/2$ and $-N/2 \leq m \leq N/2$ with the total particle number N .⁹⁵ A general form of CSS in the Dicke basis reads as^{89,98}

$$|\theta, \varphi\rangle_{CSS} = \sum_{m=-J}^J C_m(\theta) e^{-i(J+m)\varphi} |J, m\rangle, \quad (67)$$

with the coefficients

$$\begin{aligned} C_m(\theta) &= \binom{2J}{J+m}^{\frac{1}{2}} \cos^{J-m}(\theta/2) \sin^{J+m}(\theta/2), \\ &= \left[\frac{(2J)!}{(J+m)!(J-m)!} \right]^{\frac{1}{2}} \cos^{J-m}(\theta/2) \sin^{J+m}(\theta/2), \end{aligned} \quad (68)$$

which is a binomial distribution around the center θ .

One important feature of CSS is that all particles are independent and have no quantum correlations. Therefore, a CSS has equal variance $(\Delta \hat{J}_\perp)^2$ in any direction J_\perp orthogonal to the MSD (θ, φ) . The variance $(\Delta \hat{J}_\perp)^2$ is given by the sum of N variances $(\Delta \hat{S}_\perp)^2$ of individual spin- $\frac{1}{2}$ particles, that is,

$$(\Delta \hat{J}_\perp)^2 = N \times (\Delta \hat{S}_\perp)^2 = \frac{N}{4}. \quad (69)$$

Choosing the MSD along the z -axis, and the two orthogonal directions to the MSD along the x -axis and y -axis, we have

$$(\Delta \hat{J}_x)^2 = (\Delta \hat{J}_y)^2 = \frac{|\langle J_z \rangle|}{2} = \frac{N}{4}, \quad (70)$$

and

$$\Delta \hat{J}_x \Delta \hat{J}_y = \frac{|\langle J_z \rangle|}{2}. \quad (71)$$

This indicates that the CSS satisfies the minimal condition of the Heisenberg uncertainty relation, i.e., Eq. (63) takes the equal sign.

Similar to the state for a single spin- $\frac{1}{2}$ particle, $|\theta, \varphi\rangle_{CSS}$ can also be represented on a generalized Bloch sphere with a radius of the total spin length $J = N/2$. Given the polar angle θ and the azimuthal angle φ for a CSS, we have $\langle \hat{J}_x \rangle = J \cos \varphi \sin \theta$ and $\langle \hat{J}_y \rangle = J \sin \varphi \sin \theta$ and $\langle \hat{J}_z \rangle = J \cos \theta$.

The CSS can be used to perform the Ramsey interferometry.⁹⁹ The procedure of the Ramsey interferometry with a CSS is similar to the case of a single-particle state. Usually, the interferometry experiment starts from an initial state of all N atoms in the same internal state $|\downarrow\rangle$, that is, $|\Psi_0\rangle = \otimes_{i=1}^N |\downarrow\rangle_i$. Applying a $\frac{\pi}{2}$ pulse to couple the two involved internal states, one can obtain the CSS,

$$|\Psi_{in}\rangle = \otimes_{i=1}^N \left[\frac{1}{\sqrt{2}} (|\uparrow\rangle_i + |\downarrow\rangle_i) \right] \quad (72)$$

which has all atoms in the equal superposition of two internal states. Obviously, $|\Psi_{in}\rangle$ is a CSS of $\theta = \frac{\pi}{2}$ and $\varphi = 0$. Then, the system undergoes a

free evolution for a period of time, in which the ground state $|\downarrow\rangle$ accumulates a phase $\varphi/2$ and the excited state $|\uparrow\rangle$ accumulates a phase $-\varphi/2$. At the end of the free evolution, the state reads as,

$$|\Psi_{out}\rangle = \otimes_{l=1}^N \left[\frac{1}{\sqrt{2}} \left(e^{-i\frac{\varphi}{2}} |\uparrow\rangle_l + e^{+i\frac{\varphi}{2}} |\downarrow\rangle_l \right) \right]. \quad (73)$$

Finally, the second $\frac{\pi}{2}$ pulse is applied and the accumulated relative phase is extracted from the mean population difference $\langle n_{\uparrow} - n_{\downarrow} \rangle = 2 \langle \hat{J}_z \rangle$.

The evolution from the initial state $|\Psi_0\rangle$ to the final state $|\Psi_f\rangle$ is described by

$$|\Psi_f\rangle = \hat{U}|\Psi_0\rangle, \quad (74)$$

with the propagation operator^{100,101}

$$\hat{U} = \exp\left(-i\frac{\pi}{2}\hat{J}_y\right) \exp\left(-i\varphi\hat{J}_z\right) \exp\left(-i\frac{\pi}{2}\hat{J}_y\right). \quad (75)$$

Therefore, the expectation value for the final state is given by

$$\langle \hat{J}_z \rangle_f = \langle \Psi_f | \hat{J}_z | \Psi_f \rangle = \langle \Psi_0 | \hat{U}^\dagger \hat{J}_z \hat{U} | \Psi_0 \rangle. \quad (76)$$

Substituting Eq. (75) into Eq. (76), we get

$$\langle \hat{J}_z \rangle_f = -\cos\varphi \langle \hat{J}_z \rangle_0 + \sin\varphi \langle \hat{J}_y \rangle_0, \quad (77)$$

and

$$\begin{aligned} \left(\Delta \hat{J}_z\right)_f^2 &= \left(\Delta \hat{J}_z\right)_0^2 \cos^2\varphi + \left(\Delta \hat{J}_y\right)_0^2 \sin^2\varphi \\ &\quad - \sin\varphi \cos\varphi \langle \hat{J}_z \hat{J}_y + \hat{J}_y \hat{J}_z \rangle. \end{aligned} \quad (78)$$

As the initial state $|\Psi_0\rangle = \otimes_{l=1}^N |\downarrow\rangle_l$, we have

$$\langle \hat{J}_z \rangle_0 = -\frac{N}{2}, \quad \left(\Delta \hat{J}_z\right)_0 = 0, \quad \left(\Delta \hat{J}_x\right)_0 = \left(\Delta \hat{J}_y\right)_0 = \frac{\sqrt{N}}{2}. \quad (79)$$

Thus the standard deviation of the final state reads as,

$$\left(\Delta \hat{J}_z\right)_f = \frac{\sqrt{N}}{2} \sin\varphi. \quad (80)$$

Applying Eq. (3), the standard deviation of φ is given as

$$\Delta\varphi = \frac{\left(\Delta \hat{J}_z\right)_f}{\left|\partial \langle \hat{J}_z \rangle_f / \partial \varphi\right|} = \frac{1}{\sqrt{N}}. \quad (81)$$

This means that the measurement precision for the Ramsey interferometry with CSS obeys the scaling imposed by the standard quantum limit.

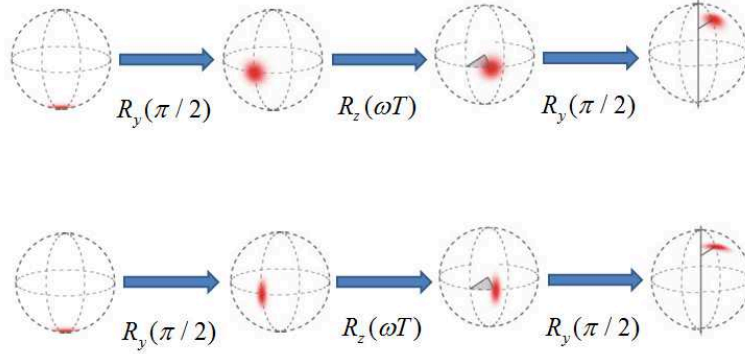


Fig. 4. Schematic diagrams of Ramsey interferometry on the Bloch sphere. Top: The initial state is a coherent spin state. Bottom: The initial state is a spin squeezed state. Adapted from Ref. 5.

4.2. Spin squeezed states

Similar to the quantum squeezing of position and momentum, without violating the Heisenberg uncertainty relation, the fluctuations of one spin component can be reduced below the symmetric limit at the expense of the increased fluctuations of the other spin component. The state of reduced spin fluctuations along a specific direction is called as spin squeezed state (SSS).^{102,103} The reduced spin fluctuations may be employed to increase the measurement precision. The occurrence of quantum spin squeezing relates to quantum entanglement among the particles.^{104–107}

There are several definitions for quantum spin squeezing.¹⁰⁸ The first squeezing parameter ξ_H is defined according to Heisenberg uncertainty relation.¹⁰⁹ It can be expressed as

$$\xi_H^2 = \frac{2(\Delta \hat{J}_\alpha)^2}{|\langle \hat{J}_\gamma \rangle|}, \alpha \neq \gamma \in (x, y, z). \quad (82)$$

A state of $\xi_H^2 < 1$ is a spin squeezed state. The second squeezing parameter ξ_S is defined by the minimum fluctuation along the direction perpendicular to the MSD.¹¹⁰ It can be written as

$$\xi_S^2 = \frac{\min(\Delta \hat{J}_{\vec{n}_\perp})^2}{j/2} = \frac{4\min(\Delta \hat{J}_{\vec{n}_\perp})^2}{N}. \quad (83)$$

Here, the minimization over all possible directions \vec{n}_\perp is to find the most squeezed direction perpendicular to the MSD. The state is supposed to

be squeezed if $\xi_S^2 < 1$. The third squeezing parameter ξ_R is defined by the ratio of the phase fluctuation for the considered state and a reference CSS.^{14,100,111} It reads as

$$\xi_R^2 = \frac{\Delta\phi}{(\Delta\phi)_{css}} = \frac{N(\Delta\hat{J}_{\vec{n}_\perp})^2}{|\langle\hat{J}\rangle|^2}. \quad (84)$$

This spin squeezing parameter is widely used in atomic Ramsey interferometry. In realistic experiments, $\Delta\hat{J}_{\vec{n}_\perp}$ can be obtained by measuring the population difference after an appropriate state rotation and $|\langle\hat{J}\rangle|$ can be extracted from the Ramsey fringes contrast. The state is spin squeezed if $\xi_R^2 < 1$.

It has demonstrated that the Ramsey interferometry with a SSS as the input state may have a higher measurement precision than the case of a CSS.¹¹² Here, we assume the initial state is a SSS of

$$\langle\hat{J}_y\rangle_0 = 0, \langle\hat{J}_z\rangle_0 = -\frac{N}{2}, (\Delta\hat{J}_y)_0 = \frac{\sqrt{N}}{2}\xi_R, \quad (85)$$

where the initial spin fluctuations are squeezed along the y -axis, i.e., the squeezing parameter $\xi_R < 1$.

Similar to the single-particle case, the interferometry with a SSS also includes two $\frac{\pi}{2}$ pulses and a free evolution. The first $\frac{\pi}{2}$ pulse rotates the initial SSS an angle $\frac{\pi}{2}$ around the y -axis. In the free evolution process, the state rotates around the z -axis with a unknown angle φ to be measured. Then applying the second $\frac{\pi}{2}$ pulse, the state rotates another $\frac{\pi}{2}$ around the y -axis. Finally, an additional rotation around its center is applied before measuring the population difference, which ensures the final population difference has minimal fluctuations.¹⁴

The evolution from the initial state to the final state can be written as

$$|\psi_f\rangle = \hat{U}|\psi_0\rangle, \quad (86)$$

with the propagation operator

$$\hat{U} = \exp(-i\frac{\pi}{2}\hat{S}_y) \exp(-i\varphi\hat{S}_z) \exp(-i\frac{\pi}{2}\hat{S}_y). \quad (87)$$

The expectation value of \hat{J}_z is given as

$$\langle\hat{J}_z\rangle_f = -\cos\varphi\langle\hat{J}_z\rangle_0 + \sin\varphi\langle\hat{J}_y\rangle_0, \quad (88)$$

and its variance reads as

$$\begin{aligned} \left(\Delta\hat{J}_z\right)_f^2 &= \left(\Delta\hat{J}_z\right)_0^2 \cos^2 \varphi + \left(\Delta\hat{J}_y\right)_0^2 \sin^2 \varphi \\ &\quad - \sin \varphi \cos \varphi \left\langle \hat{J}_z \hat{J}_y + \hat{J}_y \hat{J}_z \right\rangle. \end{aligned} \quad (89)$$

Obviously, the final state $|\psi_f\rangle$ is a SSS where the squeezed direction forms at an angle α relative to the \hat{J}_x axis. To read out \hat{J}_z with minimal uncertainty, one has to rotate the uncertainty ellipse of $|\psi_f\rangle$ around its center by an angle related to α . Therefore, without any change of the expectation value of \hat{J}_z , the readout variance of \hat{J}_z reads as

$$\left(\Delta\hat{J}_z\right)_{\text{readout}}^2 = \left(\Delta\hat{J}_y\right)_0^2. \quad (90)$$

which is given by the initial variance of \hat{J}_y . According to Eq. (3), the standard deviation of φ can be expressed as,

$$\Delta\varphi = \frac{(\Delta\hat{J}_z)_0}{\left|\partial\langle\hat{J}_z\rangle_f/\partial\varphi\right|} = \frac{\xi_R\sqrt{N}/2}{|\sin\varphi|N/2} = \frac{\xi_R}{|\sin\varphi|\sqrt{N}}. \quad (91)$$

Clearly, the measurement precision $\Delta\varphi$ reaches its minimum,

$$\Delta\varphi = \frac{\xi_R}{\sqrt{N}} \quad (92)$$

if $\varphi = \frac{\pi}{2}$. In comparison to coherent spin states, spin squeezed states may be used to beat the standard quantum limit: $\Delta\varphi \sim 1/\sqrt{N}$. For an example, if the initial state is squeezed to $\xi_R \sim 1/\sqrt{N}$, the best measurement precision can reach the Heisenberg limit: $\Delta\varphi \sim 1/N$.

4.3. NOON states

Theoretically, the NOON state has been proposed as one of the best candidates to improve the measurement precision. An NOON state is an equal-probability superposition of all N particles in mode a with zero particle in mode b , and vice versa. If the two modes are regarded as two possible paths for particles, the NOON state can be interpreted as all N particles pass through either path a or path b together, which is also called as the path-entangled state.^{42,43,74,113,114} In general, it can be written in form of

$$|NOON\rangle = \frac{1}{\sqrt{2}} (|N\rangle_a|0\rangle_b + e^{i\theta}|0\rangle_a|N\rangle_b), \quad (93)$$

with θ denoting an arbitrary phase. The NOON state is equivalent to the N -particle GHZ state, which is the maximally entangled state for a multiparticle system of two-state particles.^{115–117} For a multiparticle system involving two single-particle states $|\downarrow\rangle$ and $|\uparrow\rangle$, the N -particle GHZ state can be expressed as

$$|GHZ\rangle = \frac{1}{\sqrt{2}} \left(\left| \frac{N}{2}, +\frac{N}{2} \right\rangle + e^{i\theta} \left| \frac{N}{2}, -\frac{N}{2} \right\rangle \right), \quad (94)$$

with the Dicke basis, $|J = \frac{N}{2}, m = \frac{1}{2}(n_{\uparrow} - n_{\downarrow})\rangle$.

Below, we consider the Ramsey interferometry with,

$$|\Psi\rangle_{in} = \frac{1}{\sqrt{2}} \left(\left| \frac{N}{2}, +\frac{N}{2} \right\rangle + \left| \frac{N}{2}, -\frac{N}{2} \right\rangle \right), \quad (95)$$

as the input state before the free evolution. In the free evolution, because of the entanglement, all particles simultaneously acquire the phase shift and each particle contribute a phase shift $+\frac{\varphi}{2}$ (or $-\frac{\varphi}{2}$) corresponding to $|\downarrow\rangle$ (or $|\uparrow\rangle$). Therefore, after the free evolution, the state reads as

$$|\Psi\rangle_{out} = \frac{1}{\sqrt{2}} \left(e^{-i\frac{N\varphi}{2}} \left| \frac{N}{2}, +\frac{N}{2} \right\rangle + e^{+i\frac{N\varphi}{2}} \left| \frac{N}{2}, -\frac{N}{2} \right\rangle \right). \quad (96)$$

Below, we employ the quantum Fisher information to analyze the minimal uncertainty of measuring the phase φ . By differentiating the output state $|\Psi\rangle_{out}$ with respect to the relative phase φ , we have

$$\frac{d|\Psi\rangle_{out}}{d\varphi} = -\frac{iN}{2\sqrt{2}} \left(e^{-i\frac{N\varphi}{2}} \left| \frac{N}{2}, +\frac{N}{2} \right\rangle - e^{+i\frac{N\varphi}{2}} \left| \frac{N}{2}, -\frac{N}{2} \right\rangle \right). \quad (97)$$

According to Eq. (37), the quantum Fisher information is given as

$$F_Q^N = 4 \left[\langle \psi'(\varphi) | \psi'(\varphi) \rangle - |\langle \psi'(\varphi) | \psi(\varphi) \rangle|^2 \right] = 4 \left(\frac{N^2}{4} - 0 \right) = N^2. \quad (98)$$

Therefore, the phase uncertainty satisfies,

$$\Delta\varphi \geq \frac{1}{F_Q} = \frac{1}{N}, \quad (99)$$

which is the scaling of the Heisenberg limit. In comparison to the case of independent particles, the measurement precision is improved from the standard quantum limit to the Heisenberg limit.⁷⁵ However, in realistic experiments, it is hard to prepare a large- N GHZ state and the GHZ state is fragile in the presence of particle losses.¹¹⁸

4.4. Entangled coherent states

An entangled coherent state (ECS) is a superposition of multimode coherent states.^{119,120} A typical class of the ECS is defined as,¹²¹

$$\begin{aligned} |ECS\rangle &= e^{(-|\alpha|^2)/2} N_\alpha \sum_{n=0}^{\infty} \frac{\alpha^n}{n!} \left[(\hat{a}^\dagger)^n + (\hat{b}^\dagger)^n \right] |0\rangle_a |0\rangle_b, \\ &= N_\alpha [|\alpha\rangle_a |0\rangle_b + |0\rangle_a |\alpha\rangle_b], \end{aligned} \quad (100)$$

with the normalization factor $N_\alpha = 1/\sqrt{2(1 + e^{-|\alpha|^2})}$. This ECS can be understood as the superposition of multiple NOON states with different total particle numbers. As a coherent state involves Fock states with particle number from zero to infinity, the averaged total particle number but not the total particle number itself is a good quantity. The averaged total particle number of the ECS (100) is given by

$$\langle n \rangle = \langle n_a + n_b \rangle = 2N_\alpha^2 |\alpha|^2. \quad (101)$$

Let us consider a Mach-Zehnder interferometry with the ECS (100) as the input state for free propagation and the two modes a and b as two paths. Here, we assume that each particle in mode b acquires a phase shift φ with respect to the one in mode a . That is, the state after the free propagation reads as

$$\begin{aligned} |\Psi\rangle_{out} &= N_\alpha e^{-\frac{|\alpha|^2}{2}} \sum_{n=0}^{\infty} \frac{\alpha^n}{n!} \left[(\hat{a}^\dagger)^n + (\hat{b}^\dagger)^n e^{in\varphi} \right] |0\rangle_a |0\rangle_b \\ &= N_\alpha e^{-\frac{|\alpha|^2}{2}} \left[\left(\sum_{n=0}^{\infty} \frac{\alpha^n}{\sqrt{n!}} |n\rangle_a \right) |0\rangle_b + \left(\sum_{n=0}^{\infty} \frac{\alpha^n}{\sqrt{n!}} e^{in\varphi} |n\rangle_b \right) |0\rangle_a \right] \end{aligned} \quad (102)$$

Therefore, the derivative of the output state $|\Psi\rangle_{out}$ with respect to φ reads as

$$\frac{d|\Psi\rangle_{out}}{d\varphi} = N_\alpha \left[|0\rangle_a \left(e^{-\frac{|\alpha|^2}{2}} \sum_{n=0}^{\infty} \frac{in\alpha^n}{\sqrt{n!}} e^{in\varphi} |n\rangle_b \right) \right]. \quad (103)$$

According to Eq. (37), the quantum Fisher information is given by

$$F_Q = 4\alpha^2 N_\alpha^2 + 4(1 - N_\alpha^2)\alpha^4 N_\alpha^2. \quad (104)$$

Thus the phase uncertainty $\Delta\varphi$ satisfies

$$\Delta\varphi \geq \frac{1}{2\alpha N_\alpha \sqrt{1 + (1 - N_\alpha^2)\alpha^2}}. \quad (105)$$

If the parameters satisfy the conditions of $\alpha \gg 1$, $N_\alpha \approx 1/\sqrt{2}$ and $|\alpha|^2 \approx \langle n \rangle \gg 1$, the phase uncertainty obeys

$$\Delta\varphi \geq \frac{1}{\sqrt{2\langle n \rangle} \sqrt{1 + \langle n \rangle/2}} \approx \frac{1}{\langle n \rangle}. \quad (106)$$

This means that the phase uncertainty can approach to the Heisenberg limit.

4.5. Twin Fock states

The twin Fock state,

$$|TWIN\rangle = |N\rangle_a |N\rangle_b, \quad (107)$$

is a two-mode Fock state with equal particle number for the two modes. By using the twin Fock states as input states and parity measurements, it has been demonstrated the Heisenberg-limited Mach-Zehnder interferometry.¹²²⁻¹²⁵

The first beam splitter transforms the twin Fock state into

$$|\Psi\rangle_{BS1} = U_{BS1}|TWIN\rangle = \sum_{k=0}^N C_k^N |2k\rangle_a |2N-2k\rangle_b, \quad (108)$$

with the beam splitter operator,

$$\hat{U}_{BS1} = \exp\left[\frac{\pi}{4}(\hat{a}^\dagger \hat{b} - \hat{b}^\dagger \hat{a})\right], \quad (109)$$

and the coefficients,

$$C_k^N = \frac{1}{2^N} (-1)^{N-k} \left[\binom{2k}{k} \binom{2N-2k}{N-k} \right]^{1/2}. \quad (110)$$

Here \hat{a} and \hat{b} are the two annihilation operators for particles in modes a and b , respectively. A free propagation follows the first beam splitter, in which each particles in mode b accumulates a relative phase φ . Therefore, after the free propagation, the state reads as

$$|\Psi(\varphi)\rangle = \sum_{k=0}^N e^{i\varphi(2N-2k)} C_k^N |2k\rangle_a |2N-2k\rangle_b, \quad (111)$$

which includes the information of the phase φ to be measured. Then the second beam splitter,

$$\hat{U}_{BS2} = \exp\left[-i\frac{\pi}{4}(\hat{a}^\dagger \hat{b} + \hat{b}^\dagger \hat{a})\right], \quad (112)$$

is applied to $|\Psi(\varphi)\rangle$ and the state becomes

$$|\Psi\rangle_{out} = \hat{U}_{BS2}|\Psi(\varphi)\rangle. \quad (113)$$

Lastly, a parity measurement is performed for one of two modes. For an example, the parity operator of mode b can be expressed as

$$\hat{\Pi}_b = \exp(i\pi\hat{b}^\dagger\hat{b}), \quad (114)$$

and its expectation value is a Legendre polynomial,

$$\langle\hat{\Pi}_b\rangle = \langle\Psi|\hat{\Pi}_b|\Psi\rangle_{out} = \langle\Psi(\varphi)|\hat{U}_{BS2}^\dagger\hat{\Pi}_b\hat{U}_{BS2}|\Psi(\varphi)\rangle = P_N[\cos(2\varphi)]. \quad (115)$$

According to Eq. (3), the phase uncertainty is given by

$$\Delta\varphi = \frac{\Delta\hat{\Pi}_b}{\left|\partial\langle\hat{\Pi}_b\rangle/\partial\varphi\right|}. \quad (116)$$

For $\varphi \rightarrow 0$, the phase uncertainty $\Delta\varphi$ versus the particle number N approaches to the Heisenberg limit $\Delta\varphi_{HL} = 1/(2N)$. For other values of φ , the phase uncertainty $\Delta\varphi$ will blow up for some specific values of the total particle number and it still approaches to the Heisenberg limit for the other values of the total particle number.

The phase uncertainty can also be derived by calculating the quantum Fisher information. The derivative of $|\Psi(\varphi)\rangle$ with respect to φ reads as

$$\frac{d|\Psi(\varphi)\rangle}{d\varphi} = \sum_{k=0}^N i(2N-2k)e^{i\varphi(2N-2k)}C_k^N|2k\rangle_a|2N-2k\rangle_b. \quad (117)$$

Substituting this derivative into Eq. (37), we obtain the quantum Fisher information,

$$F_Q = 2N(1+N). \quad (118)$$

Thus the quantum Cramér-Rao bound for the phase uncertainty is given as

$$\Delta\varphi \geq \frac{1}{\sqrt{2N^2+2N}}, \quad (119)$$

which indicates that the minimal phase uncertainty obtained by the optimal measurement can reach the Heisenberg limit. This bound is consistent with the phase uncertainty obtained by the parity measurement.

5. Experimental Progresses

In recent years, there appear great advances in quantum metrology with multiparticle systems. In particular, multiparticle entangled states have been widely used to implement high-precision metrology from spectroscopy, interferometers to atomic clocks.^{126–130} To implement high-precision metrology with entangled multiparticle systems, in addition to the similar operations in quantum metrology with independent particles, a key problem is how to generate multiparticle entanglement. Usually, the multiparticle entanglement can be generated by intrinsic or artificial inter-particle interactions, such as, the intrinsic s-wave scattering between ultracold atoms, the Coulomb interaction between ultracold trapped ions, the laser-induced interaction and the continuous quantum non-demolition measurement. Below, we briefly review some typical progresses in quantum metrology with Bose-Einstein condensed atoms,^{4,5,8} ultracold trapped ions^{131,132} and cold atomic ensembles.^{6,7}

5.1. *Bose-Einstein condensed atoms*

An atomic Bose-Einstein condensate (BEC) has intrinsic atom-atom interaction dominated by the s-wave scattering, which can be used to generate entangled states such as spin squeezed states,^{133–138} GHZ states¹³⁹ and twin Fock states.^{122,125} In recent experiments, the spin squeezed states have been generated by one-axis twisting and then they are used to implement high-precision interferometry beyond the standard quantum limit.^{4,5,110,140–142} It has also been demonstrated the generation of twin Fock states via spin dynamics and the applications of the generated twin Fock states in high-precision interferometers.⁸

5.1.1. *Nonlinear interferometry with spin squeezed states*

Generally speaking, due to the intrinsic nonlinear interaction between atoms, almost all interferometers with Bose condensed atoms are nonlinear. Most of the interferometers with atomic BECs can be described by Bose-Josephson Hamiltonians. Here, for simplicity, we only discuss Bose-Josephson systems^{12,16,144–157} of Bose-Einstein condensed atoms in two different modes. There are two typical Bose-Josephson systems. One is the external Bose-Josephson junction (BJJ), which is realized by an atomic BEC in a deep double-well potential. The other is the internal BJJ, which is realized by Bose-Einstein condensed atoms involving two coupled hyper-

fine states.

The external BJJ can be described by the many-body Hamiltonian,

$$H = \int d\mathbf{r} \hat{\Psi}^\dagger(\mathbf{r}) \left[-\frac{\hbar^2 \nabla^2}{2m} + V_{dw}(\mathbf{r}) \right] \hat{\Psi}(\mathbf{r}) + \frac{g}{2} \int d\mathbf{r} \hat{\Psi}^\dagger(\mathbf{r}) \hat{\Psi}^\dagger(\mathbf{r}) \Psi(\mathbf{r}) \hat{\Psi}(\mathbf{r}), \quad (120)$$

where $\hat{\Psi}(r)$ and $\hat{\Psi}^\dagger(r)$ are bosonic field operators, $V_{dw}(\mathbf{r})$ is the double-well potential, $g = 4\pi\hbar a_s/m$, and a_s is the s-wave scattering length. By applying the two-mode approximation,¹⁵⁷ the field operator reads as,

$$\hat{\Psi}(\mathbf{r}) = \hat{b}_1 \phi_1(\mathbf{r}) + \hat{b}_2 \phi_2(\mathbf{r}), \quad (121)$$

with \hat{b}_1 and \hat{b}_2 represent the Bose annihilation operators for the atoms in the Wannier states $\phi_1(\mathbf{r})$ and $\phi_2(\mathbf{r})$, respectively.

While for an internal BJJ, it obeys the many-body quantum Hamiltonian,

$$H = \int d\mathbf{r} \left(\hat{\Psi}_1^\dagger(\mathbf{r}), \hat{\Psi}_2^\dagger(\mathbf{r}) \right) \begin{pmatrix} h_1^{(0)} & -\frac{\hbar\Omega}{2} \\ -\frac{\hbar\Omega}{2} & h_2^{(0)} \end{pmatrix} \begin{pmatrix} \hat{\Psi}_1(\mathbf{r}) \\ \hat{\Psi}_2(\mathbf{r}) \end{pmatrix} + H_{int}, \quad (122)$$

with

$$h_1^{(0)} = -\frac{\hbar^2 \nabla^2}{2m} + V_1(\mathbf{r}) - \frac{\Delta}{2},$$

$$h_2^{(0)} = -\frac{\hbar^2 \nabla^2}{2m} + V_2(\mathbf{r}) + \frac{\Delta}{2},$$

and

$$H_{int} = H_{11} + H_{22} + H_{12},$$

$$H_{11} = \frac{g_{11}}{2} \int d\mathbf{r} \hat{\Psi}_1^\dagger(\mathbf{r}) \hat{\Psi}_1^\dagger(\mathbf{r}) \Psi_1(\mathbf{r}) \hat{\Psi}_1(\mathbf{r}),$$

$$H_{22} = \frac{g_{22}}{2} \int d\mathbf{r} \hat{\Psi}_2^\dagger(\mathbf{r}) \hat{\Psi}_2^\dagger(\mathbf{r}) \Psi_2(\mathbf{r}) \hat{\Psi}_2(\mathbf{r}),$$

$$H_{12} = \frac{g_{12}}{2} \int d\mathbf{r} \hat{\Psi}_2^\dagger(\mathbf{r}) \hat{\Psi}_1^\dagger(\mathbf{r}) \Psi_1(\mathbf{r}) \hat{\Psi}_2(\mathbf{r}).$$

Here, Ω is the Rabi frequency of the coupling, Δ is the detuning to resonance, $V_j(\mathbf{r})$ denote the trapping potentials, and g_{ij} describe the s-wave scattering of atoms in modes i and j . For a spin-independent trap $V_1(\mathbf{r}) = V_2(\mathbf{r})$, assuming all atoms staying in the same spatial state $\phi(\mathbf{r})$, we can apply the two-mode approximation,

$$\hat{\Psi}_j(\mathbf{r}) = \hat{b}_j \phi(\mathbf{r}), \quad (j = 1 \text{ and } 2), \quad (123)$$

with \hat{b}_1 and \hat{b}_2 being the annihilation operators for the atoms in the two hyperfine states.

The external and internal BJJs can be described by a unified two-mode Bose-Hubbard model,¹²

$$H = -\frac{J}{2} \left(\hat{b}_2^\dagger \hat{b}_1 + \hat{b}_1^\dagger \hat{b}_2 \right) + \frac{\delta}{2} (\hat{n}_2 - \hat{n}_1) + \frac{E_c}{8} (\hat{n}_2 - \hat{n}_1)^2, \quad (124)$$

where J is the tunneling strength, δ is the imbalance and E_c is the charging energy. Obviously, $[\hat{N}, H] = 0$, therefore the total atomic number $\hat{N} = \hat{b}_1^\dagger \hat{b}_1 + \hat{b}_2^\dagger \hat{b}_2$ is conserved. By using the Fock basis $\{|n_1, n_2\rangle\}$, an arbitrary state can be expressed as $|\Psi\rangle = \sum_{n_1, n_2} C_{n_1 n_2} |n_1, n_2\rangle$, where $n_j = \hat{b}_j^\dagger \hat{b}_j$ are the number of particles in the j -th mode.

The ground state of the Hamiltonian (124) depends on all parameters.^{150,151} The competition between the Josephson tunneling and the nonlinear interaction results different ground-state behaviors. For a symmetric BJJ ($\delta = 0$), dependent on the ratio $|E_c/J|$, the system shows three different regimes: Rabi, Josephson and Fock regimes.¹⁵⁸

- In the Rabi regime, $|E_c/J| \ll N^{-1}$, the system is dominated by the Josephson term of J and there is a well defined relative phase between the two modes. The ground state is a coherent spin state, $|CSS\rangle = \exp(i\varphi \hat{J}_z) \exp(i\theta \hat{J}_y) |N/2, +N/2\rangle$.
- In the Fock regime, $|E_c/J| \gg N$, the system is dominated by the nonlinear interaction term of E_c and the relative phase between the two modes is completely random. The ground state depends on the sign of the nonlinear interaction term. If E_c is positive, the ground state is a single Fock state $|\frac{N}{2}, \frac{N}{2}\rangle$ for even N or a superposition of two Fock states $\frac{1}{\sqrt{2}} (|\frac{N}{2}, -1\rangle + |\frac{N}{2}, 1\rangle)$ for odd N . If E_c is negative, there are two degenerate ground states $|\frac{N}{2}, \frac{N}{2}\rangle$ and $|\frac{N}{2}, -\frac{N}{2}\rangle$. Therefore, any superposition of these two degenerated states including the GHZ state $\frac{1}{\sqrt{2}} (|\frac{N}{2}, \frac{N}{2}\rangle + |\frac{N}{2}, -\frac{N}{2}\rangle)$ is also a ground state. It has been proposed that the GHZ state can be adiabatically prepared and then it can be used to achieve a Heisenberg-limited interferometry.¹⁶
- In the Josephson regime, $N^{-1} \ll |E_c/J| \ll N$, the number imbalance and the relative phase are both fluctuating and the ground state is an intermediate squeezed state.

In terms of the collective spin operators (60), (61) and (62), the BJJ

Hamiltonian (124) becomes as

$$H = -B_x \hat{J}_x + B_z \hat{J}_z + \chi \hat{J}_z^2 \quad (125)$$

where the transverse magnetic field $B_x = 2J$, the longitudinal magnetic field $B_z = \delta$ and the nonlinear interaction energy $\chi = \frac{E_c}{2}$. This Hamiltonian is just the ‘one-axis twisting’ Hamiltonian for generating quantum spin squeezing.¹¹⁰ More generally, for an inter-mode coupling with Rabi frequency Ω , phase γ and detuning δ , the BJJ obeys the one-axis twisting Hamiltonian

$$H = \Omega \hat{J}_\gamma + \delta \hat{J}_z + \chi \hat{J}_z^2, \quad (126)$$

with $\hat{J}_\gamma = (\cos \gamma) \hat{J}_x - (\sin \gamma) \hat{J}_y$. Based upon this Hamiltonian, the spin squeezing of Bose condensed atoms has been demonstrated by two experimental groups: Oberthaler’s group and Treutlein’s group. They independently developed two different methods for turning on the strongly nonlinear interactions and then generating quantum spin squeezing. Oberthaler’s group has used the Feshbach resonance to decrease the inter-component s-wave scattering length.⁵ Taking into account the technical noises, the squeezing factor in this experiment⁵ can reach $\xi_N^2 = -8.2_{-1.2}^{+0.8}$ dB, which is close to the atom-loss-limited theoretical optimum for this system. Treutlein’s group has used a state-dependent trap to decrease the density overlap between two components.⁴ To obtain the best squeezing angle in their experiments, they measured the squeezing factor for different rotation angle.

(a) *The experiment with optical lattices*

By loading Bose condensed atoms into optical lattices, Oberthaler’s group has successfully prepared the entanglement of about 170 ⁸⁷Rb atoms and then realized a nonlinear Ramsey interferometer.⁵ In comparison to the ideal phase sensitivity obtained by unentangled states, their experimental data show that the phase sensitivity is enhanced by 15 percent. They firstly prepare a BEC of ⁸⁷Rb atoms occupying the hyperfine state $|F = 1, m_F = -1\rangle$ in an optical dipole trap. Then, through supposing a one-dimensional optical lattice potential, the dipole trap splits into six, which allows to perform six independent experiments in parallel. Before applying the first $\frac{\pi}{2}$ pulse, the atoms are swept from the state $|F = 1, m_F = -1\rangle$ to the state $|a\rangle = |F = 1, m_F = 1\rangle$. Since the first $\frac{\pi}{2}$ pulse, only two hyperfine states $|a\rangle = |F = 1, m_F = 1\rangle$ and $|b\rangle = |F = 2, m_F = -1\rangle$ are involved and individual systems localized in each lattice site can be

described by the one-axis twisting Hamiltonian. The effective nonlinear interaction $\chi \propto a_{aa} + a_{bb} - 2a_{ab}$ relates to the intra-species and inter-species interactions. The inter-species interaction is tuned by the Feshbach resonance and $\chi = 2\pi \times 0.063$ Hz at a magnetic field of $B = 9.10$ G. The Rabi frequency Ω can be switched rapidly from 0 to $2\pi \times 600$ Hz. Therefore, the system can be adjusted between Rabi regime and Fock regime.

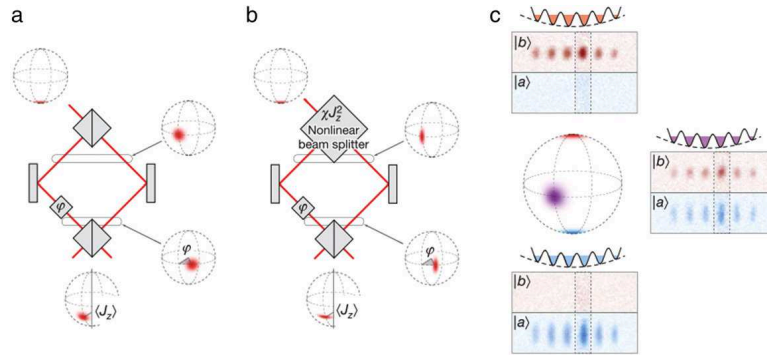


Fig. 5. (a) Schematic of a classical linear interferometer. (b) Schematic of a nonlinear interferometer. (c) Six independent BECs of ^{87}Rb in a one-dimensional optical lattice. Two-state atoms in each well form a two-mode system described by the one-axis twisting Hamiltonian. The individual detection of the condensate in each well can be achieved by high-intensity absorption imaging. From Ref. 5.

The input state for the interferometer is a coherent spin state polarized to the \hat{J}_z -direction. After the first $\pi/2$ pulse, the state rotates to the \hat{J}_x -direction, with $\langle J_z \rangle = \langle J_y \rangle = 0$ and $\Delta J_z = \Delta J_y = \sqrt{N}/2$. Then the Josephson coupling (ΩJ_γ) is switched off, the system stays in the Fock regime and its state evolves under the nonlinear term, which induces a squeezing angle α_0 with respect to z-direction. A rotation of the uncertainty ellipse around its center by $\alpha = \alpha_0 + \pi/2$ is followed. Then the modes $|a\rangle$ and $|b\rangle$ experience a $\tau = 2\mu\text{s}$ phase accumulation time and recombine via another $\pi/2$ pulse before the readout of population imbalance.

(b) The experiment with an atomic chip

By loading Bose condensed atoms into an atomic chip, Treutlein's group has created spin-squeezed states which may improve the measurement precision beyond the standard quantum limit.⁴ In the experiment, two spin states $|F = 1, m_F = -1\rangle$ and $|F = 2, m_F = 1\rangle$ of ^{87}Rb atoms are involved and the system obeys the one-axis twisting Hamiltonian (126). The effective

inter-component interaction is controlled by adjusting the spatial overlap between two spin components.

To prepare spin squeezing, except for controlling the nonlinear interaction, Treutlein's group has used similar procedures in the experiment of Oberthaler's group. First, a coherent spin state is prepared by a resonant $\frac{\pi}{2}$ pulse for $120 \mu s$. During the pulse, the coupling term dominates, $\Omega \gg \chi N$, so that the atom-atom interaction can be neglected. The state-dependent microwave potential is turned on within $50 \mu s$ to cause a sudden separation of trap minima for the two hyperfine states. The two components begin to oscillate oppositely, the overlap of the modes wavefunction reduces, which leads to the decreasing of the inter-component interaction and the increasing of effective nonlinearity χ . The nonlinearity can attain $\chi = 1.5 s^{-1}$ at the maximum separation. The two components overlap again after $12.7 ms$ and the nonlinear interaction squeezing dynamics stops.

5.1.2. *Twin matter-wave interferometry*

In addition to the quantum interferometry with spin-squeezed states, twin matter-wave interferometry with initial twin Fock states has been demonstrated in experiment.⁸ Different the spin squeezing via one-axis twisting, spin exchange dynamics of Bose condensed atoms has been used to create large ensembles of up to 10^4 pair-correlated atoms from initial twin Fock states. Attribute the pair correlation induced by spin exchange, the phase uncertainty can be beaten the standard quantum limit.

The experiment starts with creating a ^{87}Rb condensate of 2.8×10^4 atoms in the hyperfine state $|F = 2, m_F = 0\rangle$ in an optical dipole trap. Then the spin-exchange collision gradually produces correlated pairs of atoms with spins up and down. The functionality of the spin-exchange collision is just like a parametric amplifier, where the total number of the correlated pairs of atoms in $|F = 2, m_F = \pm 1\rangle$ increase exponentially with time. Afterwards, the trap is switched off and the three hyperfine states are split by a strong magnetic field gradient, and all three hyperfine states are recorded by absorption imaging. As the hyperfine states $|F = 2, m_F = \pm 1\rangle$ are generated in pairs, the number of particles in these two modes is exactly equal. Therefore, the twin Fock state is created with zero number difference and relative phase completely undetermined between these two modes.

Then the generated twin Fock state is input for implementing interferometry. The beam splitter of the interferometer is realized by three resonant microwave pulses. The first one is applied to transfer the atoms

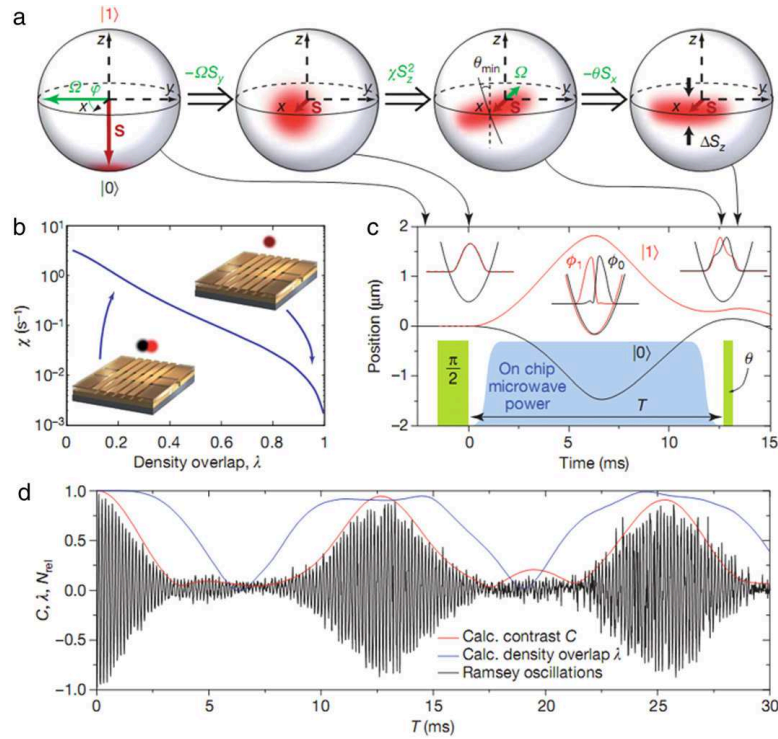


Fig. 6. (a) The preparation of spin squeezing on the generalized Bloch sphere. (b) The nonlinearity χ is decreased as the increase of the normalized density overlap λ of the two spin components. (c) The experimental sequence and the motion of two spin components corresponding to (a). (d) Measured Ramsey fringes in the normalized population difference N_{rel} . From Ref. 4.

in $|F = 2, m_F = -1\rangle$ to $|F = 1, m_F = 0\rangle$. The second pulse with duration τ couples the states $|F = 1, m_F = 0\rangle$ and $|F = 2, m_F = 1\rangle$. The third pulse transfers the atoms from $|F = 1, m_F = 0\rangle$ to $|F = 2, m_F = -1\rangle$. The action of these three pulses is equivalent to a rotation around the x -axis by an angle $\theta = \tau\Omega_R$, where Ω_R is the Rabi frequency and τ is the duration of the coupling pulse. For $\theta = \frac{\pi}{2}$, the fluctuation of the population imbalance is maximal and it corresponds to the $\pi/2$ pulse in a Ramsey interferometer or the 50:50 beam splitter in a Mach-Zehnder interferometer.

It has been demonstrated that the phase uncertainty can be enhanced beyond the standard quantum limit. The phase uncertainty $\Delta\varphi$ is inferred from the state's sensitivity to small rotation around an arbitrary axis in the xy -plane. When $\varphi \approx 0.015$ rad, the phase uncertainty can reduce to

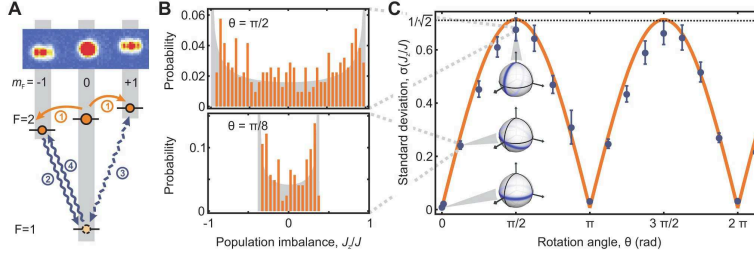


Fig. 7. (A) Schematic of the sequence of the realization of the beam splitter. Three microwave pulses are sequentially applied to achieve the coupling of the two hyperfine states $|F = 2, m_F = \pm 1\rangle$. The total effect is equivalent to a rotation around the x -axis by an angle θ . (B) Distribution of the normalized population difference for two different θ . The strongest fluctuations are obtained for $\theta = \frac{\pi}{2}$. The shaded area is the theoretical result. (C) The fluctuation of the normalized population difference versus the rotation angle θ , where the standard deviation $\sigma(J_z/J)$ oscillates approximately as $\sigma(J_z/J) = |\sin \theta|/\sqrt{2}$. From Ref. 8.

$-1.61_{-1.1}^{+0.98}$ dB, which is below the shot noise limit. If taking into account both shot noise and detection noise, the phase uncertainty can be improved to $-2.5_{-1.1}^{+0.98}$ dB.

5.2. Ultracold trapped ions

Systems of ultracold atomic ions in a Paul trap provide an excellent platform for manipulating both the internal spin and external motional degrees of freedom. Ultracold trapped ions have been proposed to explore fundamental quantum principle and implement quantum computation, quantum simulation and quantum metrology.^{22,78,159–163} Here, we give a brief introduction for some typical experiments of quantum metrology via ultracold trapped ions.

In 2001, Meyer et al. experimentally demonstrated that the sensitivity of rotation angle estimation with a Ramsey spectroscopy can be improved by using entangled trapped ions.¹³¹ The experiment used two ${}^9\text{Be}^+$ ions that are confined in a linear radio-frequency trap. Two hyperfine states $|F = 1, m_F = -1\rangle \equiv |\uparrow\rangle$ and $|F = 2, m_F = -2\rangle \equiv |\downarrow\rangle$ form the basis of an effective spin-1/2 system. $|\uparrow\rangle$ and $|\downarrow\rangle$ are coupled by two-photon Raman transitions. The detection of the ions in states $|\uparrow\rangle$ and $|\downarrow\rangle$ is done by state-sensitive fluorescence. The use of entangled states for parity measurement and Ramsey spectroscopy has been demonstrated with $|\Psi_P\rangle = (e^{i\phi}|\uparrow\uparrow\rangle + |\downarrow\downarrow\rangle)/\sqrt{2}$ and $|\Psi_R\rangle = (|\uparrow\downarrow\rangle + |\downarrow\uparrow\rangle)/\sqrt{2}$, respectively.

The experimental data show the measurement sensitivity is improved beyond the standard quantum limit (SQL) and close to the Heisenberg limit (HL).

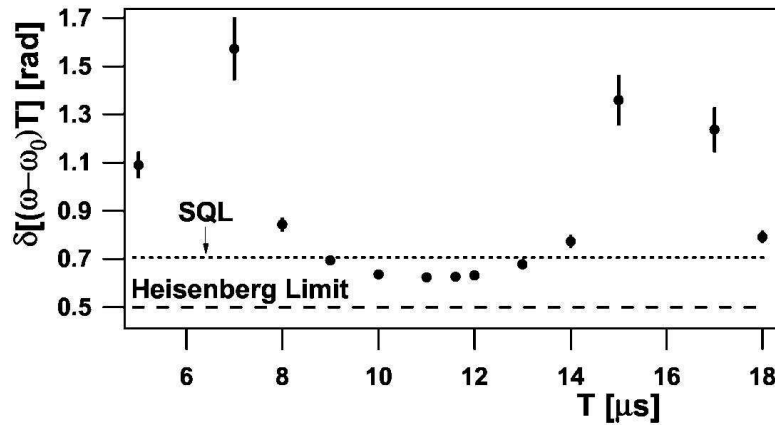


Fig. 8. Measurement precision in a Ramsey experiment with the initial state $|\Psi_R\rangle = (|\uparrow\downarrow\rangle + |\downarrow\uparrow\rangle)/\sqrt{2}$. The dotted line represent the SQL for two ions in a CSS. The dashed line is the Heisenberg limit. From Ref. 131.

Later, Leibfried et al. demonstrated the Ramsey spectroscopy with three entangled ${}^9\text{Be}^+$ ions in the GHZ state. The experimental data shows that the spectroscopic sensitivity is 1.45(2) times as high as that of a perfect experiment with three independent ions, which approaches the Heisenberg limit.¹³²

5.3. Cold atomic ensembles

In addition to the realistic inter-particle interaction, quantum non-demolition (QND) has been widely used to generate quantum spin squeezing and entanglement.^{6,7,36,164–168} It has been demonstrated that the quantum spin squeezing and entanglement for over 100 thousand cold Cs atoms can be achieved by QND measurement on the atom clock levels.^{6,7} In the experiment, the two hyperfine states $|\uparrow\rangle \equiv |F = 4, m_F = 0\rangle$ and $|\downarrow\rangle \equiv |F = 3, m_F = 0\rangle$ of Cs atoms are referred to clock levels.

The experiment is implemented as follows. Initially, by using optical pumping, the Cs atoms are prepared in the clock state $|\downarrow\rangle$. To prepare the CSS, a resonant $\pi/2$ microwave pulse at the clock frequency is applied. Then, successive QND measurements of the population difference $N_\uparrow - N_\downarrow$

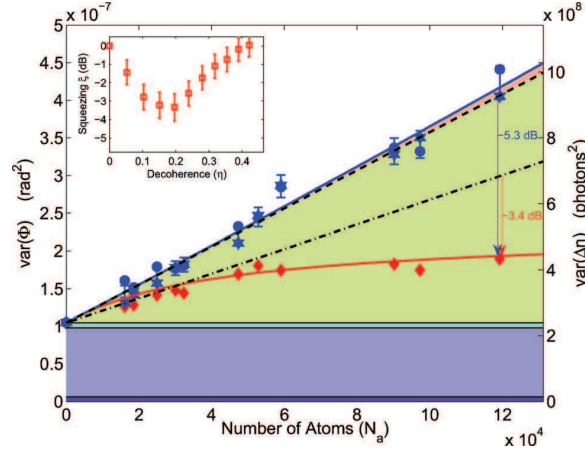


Fig. 9. Projection noise and spin squeezing via QND. Blue points, stars: variances $\text{Var}(\phi_1)$, $\text{Var}(\phi_2)$ of J_z of atoms in a CSS versus N_A ; solid blue line: quadratic fit; dashed line: CSS projection noise; red diamonds: conditionally reduced variance of a second J_z measurement predicted by the first variance; red line: reduced noise of SSS predicted from quadratic fits to projection noise data. Blue area, optical shot noise (light blue) and detector noise (dark blue); green area, projection noise. From Ref. 7.

are performed by measuring the state dependent phase shift of the off-resonant probe light in a balanced homodyne configuration. After the QND measurement, all atoms are pumped into the $F = 4$ level to determine the total atom number N_A . Two identical linear polarized beam P_\uparrow and P_\downarrow off-resonantly probe the transitions $|F = 3\rangle$ to $|F' = 4\rangle$ and $|F = 4\rangle$ to $|F' = 5\rangle$, respectively. Each beam gains a phase shift proportional to the number of atoms in the corresponding clock states,

$$\phi_\uparrow = k_\uparrow N_\uparrow, \phi_\downarrow = k_\downarrow N_\downarrow,$$

where $k_{\uparrow(\downarrow)}$ are the coupling constants and the detuning $\Delta_{\uparrow(\downarrow)}$ are tuned to make $k_\uparrow = k_\downarrow = k$. The phase difference between the two arms of the Mach-Zehnder interferometer is related to the measurement of J_z and the shot noise of the photons,

$$\phi = \frac{\delta n}{n} + 2kJ_z. \quad (127)$$

The variance of the phase difference,

$$\text{Var}(\phi) = \frac{1}{n} + k^2 \text{Var}(\Delta N). \quad (128)$$

For an atomic CSS, $\text{Var}(\Delta N) = N_A$. Finally, use n_1 photons to measure J_z to obtain a measurement result of ϕ_1 , then use n_2 photons to measure

J_z to obtain a measurement result of ϕ_2 on the same atomic ensemble can create a conditionally spin squeezed atomic state. The projection noise has been reduced to $-(5.3 \pm 0.6)$ dB and metrologically relevant spin squeezing of $-(3.4 \pm 0.7)$ dB on the Cs microwave clock transition has been realized.

6. Summary

We have given a brief introduction on quantum metrology with cold atoms both in theory and experiment. We start from the general process of physical measurements in quantum mechanics and then discuss how to estimate an unknown parameter, which is the central goal of metrology. The estimation precision is quantified by the uncertainty, which is determined by the input state, the dynamical evolution process and the readout strategy. The uncertainty of an estimated parameter is limited by the Cramér-Rao bound, which is related to the Fisher information. For a given input state and dynamical evolution, through optimizing over all possible measurements, there exists an ultimate precision limit determined by the quantum Fisher information.

To illustrate the general procedures of quantum metrology, we have introduced two typical quantum interferometry processes: Mach-Zehnder interferometry and Ramsey interferometry. The measurement precision of the interferometers with non-entangled states is limited by the standard quantum limit (SQL). By employing quantum entanglement, the SQL for the measurement precision can be surpassed by inputting multi-particle entangled states, such as, spin squeezed states, NOON states, entangled coherent states and twin Fock states. In realistic systems of cold atoms, the nonlinearity originated from intrinsic or laser induced atom-atom interactions can be used to generate various entangled states and then one can implement some particular precision measurements with the prepared entangled states.

Although there emerge great achievements in quantum metrology with cold atoms, to implement precision measurements with multi-particle entangled states and build practical quantum devices, there are still lots of important things need to be done. For an example, it is worthwhile to analyze the robustness against the environment effects. Therefore, it is vital to explore the effects to the measurement precision in the presence of dissipation, dephasing,⁹⁹ decoherence,^{74,153} temperature¹⁶⁹ and particle losses.^{94,126,170-173}

Acknowledgement

This work is supported by the NBRPC under Grant No. 2012CB821305, the NNSFC under Grants No. 11075223, the Ph.D. Programs Foundation of Ministry of Education of China under Grant No. 20120171110022, and the NCETPC under Grant No. NCET-10-0850.

References

1. J. Fortágh and C. Zimmermann, Magnetic microtraps for ultracold atoms, *Rev. Mod. Phys.* **79**, 235 (2007).
2. C. Chin, R. Grimm, P. Julienne, and E. Tiesinga, Feshbach resonances in ultracold gases, *Rev. Mod. Phys.* **82**, 1225 (2010).
3. I. Bloch, J. Dalibard, and W. Zwerger, Many-body physics with ultracold gases, *Rev. Mod. Phys.* **80**, 885 (2008).
4. M. F. Riedel, P. Bohi, Y. Li, T. W. Hansch, A. Sinatra, and P. Treutlein, Atom-chip-based generation of entanglement for quantum metrology, *Nature* **464**, 1170 (2010).
5. C. Gross, T. Zibold, E. Nicklas, J. Estve, and M. K. Oberthaler, Nonlinear atom interferometer surpasses classical precision limit, *Nature* **464**, 1165 (2010).
6. A. Louchet-Chauvet, J. Appel, J. J. Renema, D. Oblak, N. Kjaergaard, and E. S. Polzik, Entanglement-assisted atomic clock beyond the projection noise limit, *New J. Phys.* **12**, 065032 (2010).
7. J. Appel, P. J. Windpassinger, D. Oblak, U. B. Hoff, N. Kjaergaard, and E. S. Polzik, Mesoscopic atomic entanglement for precision measurements beyond the standard quantum limit, *PNAS*. **106**, 10960 (2009).
8. B. Lücke, M. Scherer, J. Kruse, L. Pezz, F. Deuretzbacher, P. Hyllus, O. Töpcü, J. Peise, W. Ertmer, J. Arlt, L. Santos, A. Smerzi, and C. Klempt, Twin matter waves for interferometry beyond the classical limit, *Science* **334**, 773 (2011).
9. V. Giovannetti, S. Lloyd, and L. Maccone, Quantum-enhanced measurements: Beating the standard quantum limit, *Science* **306**, 1330 (2004).
10. V. Giovannetti, S. Lloyd, and L. Maccone, Quantum metrology, *Phys. Rev. Lett.* **96**, 010401 (2006).
11. V. Giovannetti, S. Lloyd, and L. Maccone, Advances in quantum metrology, *Nat. Photon.* **5**, 222 (2011).
12. C. Lee, J. Huang, H. Deng, H. Dai, and J. Xu, Nonlinear quantum interferometry with Bose condensed atoms, *Front. Phys.* **7**, 109 (2012).
13. C. Gross, Spin squeezing, entanglement and quantum metrology with Bose-Einstein condensates, *J. Phys. B: At. Mol. Opt. Phys.* **45**, 103001 (2012).
14. D. J. Wineland, J. J. Bollinger, W. M. Itano, F. L. Moore, and D. J. Heinzen, Spin squeezing and reduced quantum noise in spectroscopy, *Phys. Rev. A* **46**, R6797 (1992).

15. A. Sorensen, L.-M. Duan, J. I. Cirac, and P. Zoller, Many-particle entanglement with Bose-Einstein condensates, *Nature* **409**, 63 (2001).
16. C. Lee, Adiabatic Mach-Zehnder interferometry on a quantized Bose-Josephson junction, *Phys. Rev. Lett.* **97**, 150402 (2006).
17. P. Hyllus, L. Pezzé, and A. Smerzi, Entanglement and sensitivity in precision measurements with states of a fluctuating number of particles, *Phys. Rev. Lett.* **105**, 120501 (2010).
18. L. Pezzé and A. Smerzi, Entanglement, nonlinear dynamics, and the heisenberg limit, *Phys. Rev. Lett.* **102**, 100401 (2009).
19. M. Napolitano, M. Koschorreck, B. Dubost, N. Behbood, R. J. Sewell, and M. W. Mitchell, Interaction-based quantum metrology showing scaling beyond the Heisenberg limit, *Nature* **471**, 486 (2011).
20. T. Nagata, R. Okamoto, J. L. O'Brien, K. Sasaki, and S. Takeuchi, Beating the standard quantum limit with four-entangled photons, *Science* **316**, 726 (2007).
21. C. Gross, H. Strobel, E. Nicklas, T. Zibold, N. Bar-Gill, G. Kurizki, and M. K. Oberthaler, Atomic homodyne detection of continuous-variable entangled twin-atom states, *Nature* **480**, 219 (2011).
22. Y. M. Hu, M. Feng, and C. Lee, Adiabatic Mach-Zehnder interferometer via an array of trapped ions, *Phys. Rev. A* **85**, 043604 (2012).
23. A. J. Leggett, Bose-Einstein condensation in the alkali gases: Some fundamental concepts, *Rev. Mod. Phys.* **73**, 307 (2001).
24. A. Griffin, D. W. Snoke, and S. Stringari, *Bose-Einstein Condensation*, Cambridge University Press (1995).
25. C. J. Pethick and H. Smith, *Bose-Einstein Condensation in Dilute Gases*, Cambridge University Press (2002).
26. C. F. Roos, M. Chwalla, K. Kim, M. Riebe, and R. Blatt, 'designer atoms' for quantum metrology, *Nature* **443**, 316 (2006).
27. H. Yonezawa, D. Nakane, T. A. Wheatley, K. Iwasawa, S. Takeda, H. Arao, K. Ohki, K. Tsumura, D. W. Berry, T. C. Ralph, H. M. Wiseman, E. H. Huntington, and A. Furusawa, Quantum-enhanced optical-phase tracking, *Science* **337**, 1514 (2012).
28. Y. Torii, Y. Suzuki, M. Kozuma, T. Sugiura, T. Kuga, L. Deng, and E. W. Hagley, Mach-Zehnder bragg interferometer for a Bose-Einstein condensate, *Phys. Rev. A* **61**, 041602 (2000).
29. J. J. Cooper, D. W. Hallwood, and J. A. Dunningham, Entanglement-enhanced atomic gyroscope, *Phys. Rev. A* **81**, 043624 (2010).
30. M. D. Swallows, M. Bishof, Y. Lin, S. Blatt, M. J. Martin, A. M. Rey, and J. Ye, Suppression of collisional shifts in a strongly interacting lattice clock, *Science* **331**, 1043 (2011).
31. M. J. Martin, M. Bishof, M. D. Swallows, X. Zhang, C. Benko, J. von Stecher, A. V. Gorshkov, A. M. Rey, and J. Ye, A quantum many-body spin system in an optical lattice clock, *Science* **341**, 632 (2013).
32. A. André, A. S. Sørensen, and M. D. Lukin, Stability of atomic clocks based on entangled atoms, *Phys. Rev. Lett.* **92**, 230801 (2004).
33. S. Simmons, J. A. Jones, S. D. Karlen, A. Ardavan, and J. J. L. Morton,

- Magnetic field sensors using 13-spin cat states, *Phys. Rev. A* **82**, 022330 (2010).
34. H. T. Ng, Quantum-limited measurement of magnetic-field gradient with entangled atoms, *Phys. Rev. A* **87**, 043602 (2013).
 35. W. Wasilewski, K. Jensen, H. Krauter, J. J. Renema, M. V. Balabas, and E. S. Polzik, Quantum noise limited and entanglement-assisted magnetometry, *Phys. Rev. Lett.* **104**, 133601 (2010).
 36. H. J. Kimble, Y. Levin, A. B. Matsko, K. S. Thorne, and S. P. Vyatchanin, Conversion of conventional gravitational-wave interferometers into quantum nondemolition interferometers by modifying their input and/or output optics, *Phys. Rev. D* **65**, 022002 (2001).
 37. M.-K. Zhou, Z.-K. Hu, X.-C. Duan, B.-L. Sun, J.-B. Zhao, and J. Luo, Precisely mapping the magnetic field gradient in vacuum with an atom interferometer, *Phys. Rev. A* **82**, 061602 (2010).
 38. M.-K. Zhou, Z.-K. Hu, X.-C. Duan, B.-L. Sun, L.-L. Chen, Q.-Z. Zhang, and J. Luo, Performance of a cold-atom gravimeter with an active vibration isolator, *Phys. Rev. A* **86**, 043630 (2012).
 39. H. Müntinga, H. Ahlers, M. Krutzik, A. Wenzlawski, S. Arnold, D. Becker, K. Bongs, H. Dittus, H. Duncker, N. Gaaloul, C. Gherasim, E. Giese, C. Grzeschik, T. W. Hänsch, O. Hellmig, W. Herr, S. Herrmann, E. Kajari, S. Kleinert, C. Lämmerzahl, W. Lewoczko-Adamczyk, J. Malcolm, N. Meyer, R. Nolte, A. Peters, M. Popp, J. Reichel, A. Roura, J. Rudolph, M. Schiemangk, M. Schneider, S. T. Seidel, K. Sengstock, V. Tamma, T. Valenzuela, A. Vogel, R. Walser, T. Wendrich, P. Windpassinger, W. Zeller, T. van Zoest, W. Ertmer, W. P. Schleich, and E. M. Rasel, Interferometry with Bose-Einstein condensates in microgravity, *Phys. Rev. Lett.* **110**, 093602 (2013).
 40. A.S.Holevo, *Probabilistic and statistical aspects of quantum theory* vol. 1, *North-Holland Series in Statistics and Probability*, North-Holland, North-Holland Publishing Company, Amsterdam (1982).
 41. C. M. Caves, Quantum-mechanical noise in an interferometer, *Phys. Rev. D* **23**, 1693 (1981).
 42. A. N. Boto, P. Kok, D. S. Abrams, S. L. Braunstein, C. P. Williams, and J. P. Dowling, Quantum interferometric optical lithography: Exploiting entanglement to beat the diffraction limit, *Phys. Rev. Lett.* **85**, 2733 (2000).
 43. H. Lee, P. Kok, and J. P. Dowling, A quantum rosetta stone for interferometry, *J. Mod. Opt.* **49** (2002).
 44. M. Zwiernik, C. A. Pérez-Delgado, and P. Kok, General optimality of the Heisenberg limit for quantum metrology, *Phys. Rev. Lett.* **105**, 180402 (2010).
 45. L. Maccone and V. Giovannetti, Quantum metrology: Beauty and the noisy beast, *Nat. Phys.* **7**, 376 (2011).
 46. J. H. Shapiro, S. R. Shepard, and N. C. Wong, Ultimate quantum limits on phase measurement, *Phys. Rev. Lett.* **62**, 2377 (1989).
 47. B. M. Escher, R. L. de Matos Filho, and L. Davidovich, General framework for estimating the ultimate precision limit in noisy quantum-enhanced

- metrology, *Nat. Phys.* **7**, 406 (2011).
48. Helstrom, *Quantum detection and estimation theory*, Academic Press (1976).
 49. B. W. L. Pieter Kok, *Introduction to Optical Quantum Information Processing*, Cambridge University Press (2010).
 50. S. L. Braunstein and C. M. Caves, Statistical distance and the geometry of quantum states, *Phys. Rev. Lett.* **72**, 3439 (1994).
 51. S. Boixo, S. T. Flammia, C. M. Caves, and J. Geremia, Generalized limits for single-parameter quantum estimation, *Phys. Rev. Lett.* **98**, 090401 (2007).
 52. H. Cramér, *Mathematical Methods of Statistics*, Princeton University Press (1946).
 53. S. L. Braunstein, Quantum limits on precision measurements of phase, *Phys. Rev. Lett.* **69**, 3598 (1992).
 54. R.A. Fisher, On the mathematical foundations of theoretical statistics, *Phil. Trans. R. Soc. A.* **222**, 309 (1922).
 55. R.A. Fisher, Theory of statistical estimation, *Proc. Camb. Phil. Soc.* **22**, 700 (1925).
 56. B. M. E. . R. L. de Matos Filho L. Davidovich, Quantum metrology for noisy systems, *Braz. J. Phys.* **41**, 229 (2011).
 57. M. A. Nielsen and I. L. Chuang, *Quantum Computation and Quantum Information.*, Cambridge University Press (2001).
 58. B. M. Escher, L. Davidovich, N. Zagury, and R. L. de Matos Filho, Quantum metrological limits via a variational approach, *Phys. Rev. Lett.* **109**, 190404 (2012).
 59. A. Rivas and A. Luis, Precision quantum metrology and nonclassicality in linear and nonlinear detection schemes, *Phys. Rev. Lett.* **105**, 010403 (2010).
 60. S. Boixo, A. Datta, M. J. Davis, A. Shaji, A. B. Tacla, and C. M. Caves, Quantum-limited metrology and Bose-Einstein condensates, *Phys. Rev. A* **80**, 032103 (2009).
 61. R. Demkowicz-Dobrzański, Optimal phase estimation with arbitrary *a priori* knowledge, *Phys. Rev. A* **83**, 061802 (2011).
 62. U. Dorner, R. Demkowicz-Dobrzanski, B. J. Smith, J. S. Lundeen, W. Wasilewski, K. Banaszek, and I. A. Walmsley, Optimal quantum phase estimation, *Phys. Rev. Lett.* **102**, 040403 (2009).
 63. R. Demkowicz-Dobrzanski, U. Dorner, B. J. Smith, J. S. Lundeen, W. Wasilewski, K. Banaszek, and I. A. Walmsley, Quantum phase estimation with lossy interferometers, *Phys. Rev. A* **80**, 013825 (2009).
 64. J.-W. Pan, Z.-B. Chen, C.-Y. Lu, H. Weinfurter, A. Zeilinger, and M. Żukowski, Multiphoton entanglement and interferometry, *Rev. Mod. Phys.* **84**, 777 (2012).
 65. H. F. Hofmann, All path-symmetric pure states achieve their maximal phase sensitivity in conventional two-path interferometry, *Phys. Rev. A* **79**, 033822 (2009).
 66. Z. Hradil, R. Myška, J. Peřina, M. Zawisky, Y. Hasegawa, and H. Rauch, Quantum phase in interferometry, *Phys. Rev. Lett.* **76**, 4295 (1996).
 67. S. Gasparinetti, P. Solinas, and J. P. Pekola, Geometric Landau-Zener in-

- terferometry, *Phys. Rev. Lett.* **107**, 207002 (2011).
68. L. Pezzé, A. Smerzi, G. Khoury, J. F. Hodelin, and D. Bouwmeester, Phase detection at the quantum limit with multiphoton Mach-Zehnder interferometry, *Phys. Rev. Lett.* **99**, 223602 (2007).
 69. G. A. Durkin and J. P. Dowling, Local and global distinguishability in quantum interferometry, *Phys. Rev. Lett.* **99**, 070801 (2007).
 70. N. F. Ramsey, A molecular beam resonance method with separated oscillating fields, *Phys. Rev.* **78**, 695 (1950).
 71. N. F. Ramsey, A new molecular beam resonance method, *Phys. Rev.* **76**, 996 (1949).
 72. I. I. Rabi, S. Millman, P. Kusch, and J. R. Zacharias, The molecular beam resonance method for measuring nuclear magnetic moments. the magnetic moments of ${}^3\text{Li}^6$, ${}^3\text{Li}^7$ and ${}^9\text{F}^{19}$, *Phys. Rev.* **55**, 526 (1939).
 73. C. J. Foot, *Atomic Physics*, Oxford University Press (2005).
 74. G. Ferrini, D. Spehner, A. Minguzzi, and F. W. J. Hekking, Effect of phase noise on quantum correlations in Bose-Josephson junctions, *Phys. Rev. A* **84**, 043628 (2011).
 75. M. J. Holland and K. Burnett, Interferometric detection of optical phase shifts at the heisenberg limit, *Phys. Rev. Lett.* **71**, 1355 (1993).
 76. D. W. Berry, H. M. Wiseman, and J. K. Breslin, Optimal input states and feedback for interferometric phase estimation, *Phys. Rev. A* **63**, 053804 (2001).
 77. L. Pezzé and A. Smerzi, Ultrasensitive two-mode interferometry with single-mode number squeezing, *Phys. Rev. Lett.* **110**, 163604 (2013).
 78. D. Leibfried, B. DeMarco, V. Meyer, M. Rowe, A. Ben-Kish, J. Britton, W. M. Itano, B. Jelenković, C. Langer, T. Rosenband, and D. J. Wineland, Trapped-ion quantum simulator: Experimental application to nonlinear interferometers, *Phys. Rev. Lett.* **89**, 247901 (2002).
 79. L. Pezzé and A. Smerzi, Phase sensitivity of a Mach-Zehnder interferometer, *Phys. Rev. A* **73**, 011801 (2006).
 80. M. B. Serge Haroche and J.-M. Raimond, Atomic clocks for controlling light fields, *Phys. Today* **66**, 27 (2013).
 81. D. Kleppner, Norman ramsey and his method, *Phys. Today* **66**, 25 (2013).
 82. N. F. Ramsey, The method of successive oscillatory fields, *Phys. Today* **66**, 36 (2013).
 83. J. J. Bollinger, W. M. Itano, D. J. Wineland, and D. J. Heinzen, Optimal frequency measurements with maximally correlated states, *Phys. Rev. A* **54**, R4649 (1996).
 84. D. W. Berry and H. M. Wiseman, Optimal states and almost optimal adaptive measurements for quantum interferometry, *Phys. Rev. Lett.* **85**, 5098 (2000).
 85. H. Cable and G. A. Durkin, Parameter estimation with entangled photons produced by parametric down-conversion, *Phys. Rev. Lett.* **105**, 013603 (2010).
 86. K. P. Seshadreesan, P. M. Anisimov, H. Lee, and J. P. Dowling, Parity detection achieves the Heisenberg limit in interferometry with coherent mixed

- with squeezed vacuum light, *New J. Phys.* **13** (2011).
87. Y. Ben-Aryeh, Phase estimation by photon counting measurements in the output of a linear Mach-Zehnder interferometer, *J. Opt. Soc. Am. B.* **29**, 2754 (2012).
 88. P. M. Anisimov, G. M. Raterman, A. Chiruvelli, W. N. Plick, S. D. Huver, H. Lee, and J. P. Dowling, Quantum metrology with two-mode squeezed vacuum: Parity detection beats the Heisenberg limit, *Phys. Rev. Lett.* **104**, 103602 (2010).
 89. X. Wang and B. C. Sanders, Relations between bosonic quadrature squeezing and atomic spin squeezing, *Phys. Rev. A* **68**, 033821 (2003).
 90. J. Kong, Z. Y. Ou, and W. Zhang, Phase-measurement sensitivity beyond the standard quantum limit in an interferometer consisting of a parametric amplifier and a beam splitter, *Phys. Rev. A* **87**, 023825 (2013).
 91. L.-M. Kuang and X. Chen, Phase-coherent states and their squeezing properties, *Phys. Rev. A* **50**, 4228 (1994).
 92. A. M. Dudarev, R. B. Diener, B. Wu, M. G. Raizen, and Q. Niu, Entanglement generation and multiparticle interferometry with neutral atoms, *Phys. Rev. Lett.* **91**, 010402 (2003).
 93. S. F. Huelga, C. Macchiavello, T. Pellizzari, A. K. Ekert, M. B. Plenio, and J. I. Cirac, Improvement of frequency standards with quantum entanglement, *Phys. Rev. Lett.* **79**, 3865 (1997).
 94. S. D. Huver, C. F. Wildfeuer, and J. P. Dowling, Entangled Fock states for robust quantum optical metrology, imaging, and sensing, *Phys. Rev. A* **78**, 063828 (2008).
 95. F. T. Arecchi, E. Courtens, R. Gilmore, and H. Thomas, Atomic coherent states in quantum optics, *Phys. Rev. A* **6**, 2211 (1972).
 96. J. J. Sakurai, *Modern Quantum Mechanics*, New York: Addison-Wesley (1993).
 97. J. M. Radcliffe, Some properties of coherent spin states, *J. Phys. A.* **4**, 313 (1971).
 98. W.-M. Zhang, D. H. Feng, and R. Gilmore, Coherent states: Theory and some applications, *Rev. Mod. Phys.* **62**, 867 (1990).
 99. Y. C. Liu, G. R. Jin, and L. You, Quantum-limited metrology in the presence of collisional dephasing, *Phys. Rev. A* **82**, 045601 (2010).
 100. D. J. Wineland, J. J. Bollinger, W. M. Itano, and D. J. Heinzen, Squeezed atomic states and projection noise in spectroscopy, *Phys. Rev. A* **50**, 67 (1994).
 101. T. Kim, O. Pfister, M. J. Holland, J. Noh, and J. L. Hall, Influence of decorrelation on Heisenberg-limited interferometry with quantum correlated photons, *Phys. Rev. A* **57**, 4004 (1998).
 102. D. F. Walls, Squeezed states of light, *Nature* **306**, 141 (1983).
 103. C. A. Sackett, Quantum measurement: A condensate's main squeeze, *Nature* **464**, 1133 (2010).
 104. M. Hillery and M. S. Zubairy, Entanglement conditions for two-mode states, *Phys. Rev. Lett.* **96**, 050503 (2006).
 105. X. Wang and B. C. Sanders, Spin squeezing and pairwise entanglement for

- symmetric multiqubit states, *Phys. Rev. A* **68**, 012101 (2003).
106. G.-R. Jin and S. W. Kim, Storage of spin squeezing in a two-component Bose-Einstein condensate, *Phys. Rev. Lett.* **99**, 170405 (2007).
 107. A. S. Sørensen and K. Mølmer, Entanglement and extreme spin squeezing, *Phys. Rev. Lett.* **86**, 4431 (2001).
 108. J. Ma, X. Wang, C. Sun, and F. Nori, Quantum spin squeezing, *Physics Reports* **509**, 89 (2011).
 109. D. F. Walls and P. Zoller, Reduced quantum fluctuations in resonance fluorescence, *Phys. Rev. Lett.* **47**, 709 (1981).
 110. M. Kitagawa and M. Ueda, Squeezed spin states, *Phys. Rev. A* **47**, 5138 (1993).
 111. X. Wang, A. Søndberg Sørensen, and K. Mølmer, Spin squeezing in the Ising model, *Phys. Rev. A* **64**, 053815 (2001).
 112. D. Ulam-Orgikh and M. Kitagawa, Spin squeezing and decoherence limit in ramsey spectroscopy, *Phys. Rev. A* **64**, 052106 (2001).
 113. D. Meiser and M. J. Holland, Robustness of Heisenberg-limited interferometry with balanced fock states, *New J. Phys.* **11**, 033002 (2009).
 114. K. Banaszek, R. Demkowicz-Dobrzanski, and I. A. Walmsley, Quantum states made to measure, *Nat. Photon.* **3**, 673 (2009).
 115. Z. Ji, G. Wang, R. Duan, Y. Feng, and M. Ying, Parameter estimation of quantum channels, *IEEE TRANSACTIONS ON INFORMATION THEORY* **54**, 5172 (2008).
 116. A. Shaji and C. M. Caves, Qubit metrology and decoherence, *Phys. Rev. A* **76**, 032111 (2007).
 117. G. Meng, H. Xu, S. Yang, S. Zhang, G. Guo, B. Shi, and X. Zou, Fast generation of many-atom maximal entanglement in spin-1 Bose-Einstein condensates, *Phys. Rev. A* **85**, 035601 (2012).
 118. I. Afek, O. Ambar, and Y. Silberberg, High-NOON states by mixing quantum and classical light, *Science* **328**, 879 (2010).
 119. B. C. Sanders, Review of entangled coherent states, *J. Phys. A* **45**, 244002 (2012).
 120. B. C. Sanders, Entangled coherent states, *Phys. Rev. A* **45**, 6811 (1992).
 121. J. Joo, W. J. Munro, and T. P. Spiller, Quantum metrology with entangled coherent states, *Phys. Rev. Lett.* **107**, 083601 (2011).
 122. C. C. Gerry and J. Mimih, Heisenberg-limited interferometry with pair coherent states and parity measurements, *Phys. Rev. A* **82**, 013831 (2010).
 123. J. A. Dunningham, K. Burnett, and S. M. Barnett, Interferometry below the standard quantum limit with Bose-Einstein condensates, *Phys. Rev. Lett.* **89**, 150401 (2002).
 124. R. A. Campos, C. C. Gerry, and A. Benmoussa, Optical interferometry at the Heisenberg limit with twin fock states and parity measurements, *Phys. Rev. A* **68**, 023810 (2003).
 125. J. A. Dunningham and K. Burnett, Sub-shot-noise-limited measurements with Bose-Einstein condensates, *Phys. Rev. A* **70**, 033601 (2004).
 126. Y. Li, P. Treutlein, J. Reichel, and A. Sinatra, Spin squeezing in a bimodal condensate: spatial dynamics and particle losses, *Eur. Phys. J. B* **68**, 365

- (2009).
127. R. Bucker, J. Grond, S. Manz, T. Berrada, T. Betz, C. Koller, U. Hohenester, T. Schumm, A. Perrin, and J. Schmiedmayer, Twin-atom beams, *Nat. Phys.* **7**, 608 (2011).
 128. J. J. Cooper, D. W. Hallwood, J. A. Dunningham, and J. Brand, Robust quantum enhanced phase estimation in a multimode interferometer, *Phys. Rev. Lett.* **108**, 130402 (2012).
 129. M. Rab, A. L. C. Hayward, J. H. Cole, A. D. Greentree, and A. M. Martin, Interferometry using adiabatic passage in dilute-gas Bose-Einstein condensates, *Phys. Rev. A* **86**, 063605 (2012).
 130. J. Grond, U. Hohenester, J. Schmiedmayer, and A. Smerzi, Mach-Zehnder interferometry with interacting trapped Bose-Einstein condensates, *Phys. Rev. A* **84**, 023619 (2011).
 131. V. Meyer, M. A. Rowe, D. Kielpinski, C. A. Sackett, W. M. Itano, C. Monroe, and D. J. Wineland, Experimental demonstration of entanglement-enhanced rotation angle estimation using trapped ions, *Phys. Rev. Lett.* **86**, 5870 (2001).
 132. D. Leibfried, M. D. Barrett, T. Schaetz, J. Britton, J. Chiaverini, W. M. Itano, J. D. Jost, C. Langer, and D. J. Wineland, Toward Heisenberg-limited spectroscopy with multiparticle entangled states, *Science* **304**, 1476 (2004).
 133. I. M. Julian Grond, Ulrich Hohenester and J. Schmiedmayer, Atom interferometry with trapped Bose-Einstein condensates: impact of atom-atom interactions, *New J. Phys.* **12**, 065036 (2010).
 134. C. Orzel, A. K. Tuchman, M. L. Fenselau, M. Yasuda, and M. A. Kasevich, Squeezed states in a Bose-Einstein condensate, *Science* **291**, 2386 (2001).
 135. J. Esteve, C. Gross, A. Weller, S. Giovanazzi, and M. K. Oberthaler, Squeezing and entanglement in a Bose-Einstein condensate, *Nature* **455**, 1216 (2008).
 136. C. Bodet, J. Estève, M. K. Oberthaler, and T. Gasenzer, Two-mode Bose gas: Beyond classical squeezing, *Phys. Rev. A* **81**, 063605 (2010).
 137. B. Zeng, D. L. Zhou, Z. Xu, and L. You, Entanglement and spin-squeezing properties for three bosons in two modes, *Phys. Rev. A* **71**, 042317 (2005).
 138. O. E. Müstecaplıoğlu, M. Zhang, and L. You, Spin squeezing and entanglement in spinor condensates, *Phys. Rev. A* **66**, 033611 (2002).
 139. L. You, Creating maximally entangled atomic states in a Bose-Einstein condensate, *Phys. Rev. Lett.* **90**, 030402 (2003).
 140. S. Boixo, A. Datta, M. J. Davis, S. T. Flammia, A. Shaji, and C. M. Caves, Quantum metrology: Dynamics versus entanglement, *Phys. Rev. Lett.* **101**, 040403 (2008).
 141. Y.-C. Liu, G.-R. Jin, and W.-M. Liu, Spin squeezing in a generalized one-axis twisting model, *New J. Phys.* **11**, 073049 (2009).
 142. Y. C. Liu, Z. F. Xu, G. R. Jin, and L. You, Spin squeezing: Transforming one-axis twisting into two-axis twisting, *Phys. Rev. Lett.* **107**, 013601 (2011).
 143. Y. Khodorkovsky, G. Kurizki, and A. Vardi, Decoherence and entanglement in a bosonic Josephson junction Bose-enhanced quantum Zeno control of

- phase diffusion, *Phys. Rev. A* **80**, 023609 (2009).
144. A. Smerzi, S. Fantoni, S. Giovanazzi, and S. R. Shenoy, Quantum coherent atomic tunneling between two trapped Bose-Einstein condensates, *Phys. Rev. Lett.* **79**, 4950 (1997).
 145. G. J. Milburn, J. Corney, E. M. Wright, and D. F. Walls, Quantum dynamics of an atomic Bose-Einstein condensate in a double-well potential, *Phys. Rev. A* **55**, 4318 (1997).
 146. M. J. Steel and M. J. Collett, Quantum state of two trapped Bose-Einstein condensates with a Josephson coupling, *Phys. Rev. A* **57**, 2920 (1998).
 147. R. W. Spekkens and J. E. Sipe, Spatial fragmentation of a Bose-Einstein condensate in a double-well potential, *Phys. Rev. A* **59**, 3868 (1999).
 148. C. Lee, W. Hai, L. Shi, X. Zhu, and K. Gao, Chaotic and frequency-locked atomic population oscillations between two coupled Bose-Einstein condensates, *Phys. Rev. A* **64**, 053604 (2001).
 149. C. Lee, W. Hai, L. Shi, and K. Gao, Phase-dependent spontaneous spin polarization and bifurcation delay in coupled two-component Bose-Einstein condensates, *Phys. Rev. A* **69**, 033611 (2004).
 150. R. Gati and M. K. Oberthaler, A bosonic Josephson junction, *J. Phys. B* **40**, R61 (2007).
 151. C. Lee, L.-B. Fu, and Y. S. Kivshar, Many-body quantum coherence and interaction blockade in Josephson-linked Bose-Einstein condensates, *EPL* **81**, 60006 (2008).
 152. L.-B. Fu, D.-F. Ye, C. Lee, W. Zhang, and J. Liu, Adiabatic Rosen-Zener interferometry with ultracold atoms, *Phys. Rev. A* **80**, 013619 (2009).
 153. N. Bar-Gill, G. Kurizki, M. Oberthaler, and N. Davidson, Dynamic control and probing of many-body decoherence in double-well Bose-Einstein condensates, *Phys. Rev. A* **80**, 053613 (2009).
 154. C. Lee, Universality and anomalous mean-field breakdown of symmetry-breaking transitions in a coupled two-component condensate, *Phys. Rev. Lett.* **102**, 070401 (2009).
 155. Q. Y. He, M. D. Reid, T. G. Vaughan, C. Gross, M. Oberthaler, and P. D. Drummond, Einstein-Podolsky-Rosen entanglement strategies in two-well Bose-Einstein condensates, *Phys. Rev. Lett.* **106**, 120405 (2011).
 156. H. T. Ng and S.-I. Chu, Steady-state entanglement in a double-well Bose-Einstein condensate through coupling to a superconducting resonator, *Phys. Rev. A* **84**, 023629 (2011).
 157. B. Dalton and S. Ghanbari, Two-mode theory of Bose-Einstein condensates: interferometry and the Josephson model, *J. Mod. Opt.* **59**, 287 (2012).
 158. O. E. Müstecaplıoğlu, W. Zhang, and L. You, Quantum dynamics of a spin-1 condensate in a double-well potential, *Phys. Rev. A* **75**, 023605 (2007).
 159. H. Häffner, S. Gulde, M. Riebe, G. Lancaster, C. Becher, J. Eschner, F. Schmidt-Kaler, and R. Blatt, Precision measurement and compensation of optical Stark shifts for an ion-trap quantum processor, *Phys. Rev. Lett.* **90**, 143602 (2003).
 160. A. Bermudez, P. O. Schmidt, M. B. Plenio, and A. Retzker, Robust trapped-ion quantum logic gates by continuous dynamical decoupling, *Phys. Rev. A*

- 85**, 040302 (2012).
161. A. Stute, B. Casabone, P. Schindler, T. Monz, P. O. Schmidt, B. Brandstatter, T. E. Northup, and R. Blatt, Tunable ion-photon entanglement in an optical cavity, *Nature* **485**, 482 (2012).
 162. B. B. Blinov, D. L. Moehring, L.-M. Duan, and C. Monroe, Observation of entanglement between a single trapped atom and a single photon, *Nature* **428**, 153 (2004).
 163. J. Volz, M. Weber, D. Schlenk, W. Rosenfeld, J. Vrana, K. Saucke, C. Kurtsiefer, and H. Weinfurter, Observation of entanglement of a single photon with a trapped atom, *Phys. Rev. Lett.* **96**, 030404 (2006).
 164. Z. Chen, J. G. Bohnet, S. R. Sankar, J. Dai, and J. K. Thompson, Conditional spin squeezing of a large ensemble via the vacuum rabi splitting, *Phys. Rev. Lett.* **106**, 133601 (2011).
 165. H. Krauter, C. A. Muschik, K. Jensen, W. Wasilewski, J. M. Petersen, J. I. Cirac, and E. S. Polzik, Entanglement generated by dissipation and steady state entanglement of two macroscopic objects, *Phys. Rev. Lett.* **107**, 080503 (2011).
 166. A. Kuzmich, L. Mandel, and N. P. Bigelow, Generation of spin squeezing via continuous quantum nondemolition measurement, *Phys. Rev. Lett.* **85**, 1594 (2000).
 167. J. Hald, J. L. Sørensen, C. Schori, and E. S. Polzik, Spin squeezed atoms: A macroscopic entangled ensemble created by light, *Phys. Rev. Lett.* **83**, 1319 (1999).
 168. C. M. Trail, P. S. Jessen, and I. H. Deutsch, Strongly enhanced spin squeezing via quantum control, *Phys. Rev. Lett.* **105**, 193602 (2010).
 169. A. Sinatra, E. Witkowska, and Y. Castin, Spin squeezing in finite temperature Bose-Einstein condensates: Scaling with the system size, *The European Physical Journal Special Topics*. **203**, 87 (2012).
 170. X.-X. Zhang, Y.-X. Yang, and X.-B. Wang, Lossy quantum-optical metrology with squeezed states, *Phys. Rev. A* **88**, 013838 (2013).
 171. A. Datta, L. Zhang, N. Thomas-Peter, U. Dorner, B. J. Smith, and I. A. Walmsley, Quantum metrology with imperfect states and detectors, *Phys. Rev. A* **83**, 063836 (2011).
 172. L. Maccone and G. De Cillis, Robust strategies for lossy quantum interferometry, *Phys. Rev. A* **79**, 023812 (2009).
 173. N. Spagnolo, C. Vitelli, V. G. Lucivero, V. Giovannetti, L. Maccone, and F. Sciarrino, Phase estimation via quantum interferometry for noisy detectors, *Phys. Rev. Lett.* **108**, 233602 (2012).